A&A 541, A97 (2012)
DOI: 10.1051/0004-6361/201117350

Astronomy & Astrophysics

Extrasolar planet population synthesis

IV. Correlations with disk metallicity, mass, and lifetime

C. Mordasini[1], Y. Alibert[2,3], W. Benz[2], H. Klahr[1], and T. Henning[1]

[1] Max-Planck-Institut für Astronomie, Königstuhl 17, 69117 Heidelberg, Germany
e-mail: mordasini@mpia.de
[2] Physikalisches Institut, University of Bern, Sidlerstrasse 5, 3012 Bern, Switzerland
[3] Institut UTINAM, CNRS-UMR 6213, Observatoire de Besançon, BP 1615, 25010 Besançon Cedex, France

Received 27 May 2011 / Accepted 27 December 2011

ABSTRACT

Context. This is the fourth paper in a series showing the results of planet population synthesis calculations. In Paper I, we presented our methods. In Paper II, we compared the synthetic and the observed planetary population statistically. Paper III addressed the influences of the stellar mass on the population.
Aims. Our goal in this fourth paper is to systematically study the effects of important disk properties, namely disk metallicity, mass, and lifetime on fundamental properties of planets like mass and semimajor axis.
Methods. For a large number of protoplanetary disks that have properties following distributions derived from observations, we calculated a population of planets with our formation model. The model is based on the classical core accretion paradigm but self-consistently includes planet migration and disk evolution.
Results. We find a very large number of correlations. Regarding the planetary initial mass function, metallicity, $M_{\rm disk}$, and $\tau_{\rm disk}$ play different roles. For high metallicities, giant planets are more frequent. For high $M_{\rm disk}$, giant planets are more massive. For long $\tau_{\rm disk}$, giant planets are both more frequent and massive. At low metallicities, very massive giant planets cannot form, but otherwise giant planet mass and metallicity are nearly uncorrelated. In contrast, (maximum) planet masses and disk gas masses are correlated. The formation of giant planets is possible for initial planetesimal surface densities $\Sigma_{\rm S}$ of at least 6 g/cm^2 at 5.2 AU. The best spot for giant planet formation is at ∼5 AU. In- and outside this distance, higher $\Sigma_{\rm S}$ are necessary. Low metallicities can be compensated for by high $M_{\rm disk}$, and vice versa, but not ad infinitum. At low metallicities, giant planets only form outside the ice line, while giant planet formation occurs throughout the disk at high metallicities. The extent of migration increases with $M_{\rm disk}$ and $\tau_{\rm disk}$ and usually decreases with metallicity. No clear correlation of metallicity and the semimajor axis distribution of giant planets exists because in low-metallicity disks, planets start farther out, but migrate more, while the contrary applies to high metallicities. The final semimajor axis distribution contains an imprint of the ice line. Close-in low mass planets have a lower mean metallicity than hot Jupiters. The frequency of giant planets varies approximately as $M_{\rm disk}^{1.2}$ and $\tau_{\rm disk}^2$.
Conclusions. The properties of protoplanetary disks – the initial and boundary conditions for planet formation – are decisive for the properties of planets, and leave many imprints on the population.

Key words. planetary systems – protoplanetary disks – planets and satellites: formation – planet-disk interactions

1. Introduction

The number of known extrasolar planets has grown large enough to look at the statistical properties of the population as a whole, rather than at the properties of single objects, and to compare the actual population with a synthetic population obtained from a theoretical planet formation model. In this way *all* discovered planets serve (provided the detection bias is known) to constrain the model, and to improve our understanding of planet formation. We used our extended core accretion formation model (Alibert et al. 2005a) to generate populations of synthetic extrasolar planets (Mordasini et al. 2009a, hereafter Paper I) with the Monte Carlo method. Then, we compared the detectable synthetic planets with an observational comparison sample of actual exoplanets using statistical methods (Mordasini et al. 2009b, hereafter Paper II). We found that we could reproduce in a statistically significant way some of the most important properties of the observed extrasolar giant planets. Finally, in Alibert et al. (2010, hereafter Paper III), we discussed the influence of the stellar mass on the synthetic planetary population, studying for example the effect on the planetary initial mass function, the semimajor axis distribution, or the "metallicity effect" (the increase in the detection probability of giant planets with metallicity). In this Paper IV, we again focus on solar-like stars.

Over the last few years, considerable observational progress has been achieved in characterizing the end products of planetary formation process, i.e. the planet themselves. Progress has also been substantial in characterizing the initial and boundary conditions for this process, i.e. the properties of protoplanetary disks. This was made possible in a large measure by new observational facilities like *Spitzer* (e.g. Fang et al. 2009). Observations of disks around young stars have provided us with knowledge of the distributions of disk masses (Beckwith & Sargent 1996; Andrews et al. 2009), disk sizes (McCaughrean & Odell 1996; Andrews et al. 2010), and lifetimes (Haisch et al. 2001; Fedele et al. 2010). Additionally, correlations between disk properties and stellar mass were discovered (Kennedy & Kenyon 2009; Mamajek 2009) that have important implications for the formation of planets around stars of different masses (Currie 2009; Paper III). As shown in Paper I, the diversity of

extrasolar planets is a direct consequence of the diversity of protoplanetary disks, which means that the properties of disks are critical in defining the outcome of planet formation in such disks.

In this article we focus on correlations between disk and planetary properties. We study systematically the influences of disk metallicity [Fe/H], disk (gas) mass $M_{\rm disk}$, and lifetime $\tau_{\rm disk}$ on important, observable properties of synthetic planets by computing several models of planet formation.

1.1. Observed correlations

From an observational point of view, a number of correlations were inferred in the past years, with various degrees of significance (see Udry & Santos 2007; or Mayor et al. 2011, for an overview). We address in this paper the following correlations.

(1) The clearest correlation is the link between the stellar metallicity (to first order an indicator of the initial dust-to-gas-ratio in the disk, see Santos et al. 2003) and the likelihood of detecting a giant planet. This "metallicity effect" has been observationally known for a long time and is very well established for solar-like stars by numerous studies (e.g. Gonzalez 1997; Santos et al. 2001; Fischer & Valenti 2005; Udry & Santos 2007). The "metallicity effect" was studied as an observational constraint in Paper II and is here further addressed in Sects. 4.2, 4.3, and 8.1.
(2) Interestingly, lower mass Neptunian and super-Earth planets seem, in contrast, not to be found primarily around high [Fe/H] stars (Mayor & Udry 2008; Sousa et al. 2008; Ghezzi et al. 2010a). We study this in Sects. 4.1 and 7.
(3) Already much less compelling is the possible absence of very massive planets (in a mass range of about 5 to 20 Jupiter masses, $M_{\rm J}$) orbiting within a few AUs low-metallicity, solar-like stars as found in radial velocity (RV) searches. This possible absence was noted by Udry et al. (2002), Santos et al. (2003), and Fischer & Valenti (2005), and is discussed in Sect. 4.3.3.
(4) In contrast, no secure correlations have been found between stellar metallicity and the planetary semimajor axis, at least among RV detections (Udry & Santos 2007; Valenti & Fischer 2008; Ammler-von Eiff et al. 2009), even though possible correlations have been discussed in the literature. Sozzetti (2004), for example, studied whether stars with Pegasi planets have particularly high [Fe/H], even among planet hosts. Correlations between migration, semimajor axis, and metallicity are addressed in Sects. 6.1 and 6.3.
(5) Giant planets are more frequently found orbiting A stars than orbiting solar-like stars, and are also more massive (Lovis & Mayor 2007; Bowler et al. 2010) on average. In Paper III it was shown that this correlation can be reproduced best if one assumes a roughly linear scaling between disk (gas) mass and stellar mass. This implies, at least partially, a correlation between disk mass and planet mass (Sects. 4.1.2 and 4.4).

In addition, we address several other correlations below that appear in the models but that have not yet been reported in the observation, but they could become observable in the future with better instruments and larger, more complete data bases.

1.2. Special role of [Fe/H]

Population synthesis is a powerful tool for investigating such correlations, because all properties of the (numerical) parent disks, and those of the synthetic planet populations emerging from them are known. For actual exoplanets, this is obviously not the case. Observationally, the host stars metallicity can only be determined and assumed to be a proxy for the disks dust-to-gas ratio $f_{\rm D/G}$. Other fundamental parameters of the disks, such as their initial gas mass (which together with $f_{\rm D/G}$ sets the absolute amount of solids) and their lifetime, cannot be observationally determined. It is therefore no surprise that the observationally inferred correlations essentially involve only the metallicity.

A recently discussed correlation that could partially change this is the possible enhanced lithium depletion measured in Sun-like stars hosting planets (Israelian et al. 2009; but see Baumann et al. 2010, for an opposed view). This is because such a depletion could result from a positive correlation of disk lifetime and likelihood of forming giant planets (Bouvier 2008). The influence of the disk lifetime $\tau_{\rm disk}$ on the occurrence of giant planets, as observed in our models, is discussed in Sect. 8.3.

In general, however, only probability distributions for disk masses and lifetimes can be inferred from the observations of star-forming regions. Our study to a certain degree allows narrowing down these probability distributions for a specific star-planet system, since not all types of planets can form in all types of disks.

1.3. Earlier works

Several studies have already addressed correlations between disk and planetary properties. Ida & Lin (2004b) studied the influences of the metallicity as modeled by the dust-to-gas ratio. They find that the normalized mass and semimajor axis distributions of the potentially observable (giant) synthetic planets are fairly independent of [Fe/H], while the frequency of giant planets increases with it, in agreement with observations. Kornet et al. (2005) modeled the evolution of the solids from dust size to planetesimals and, using the final planetesimal surface density, estimated the capability to form giant planets. Such an approach also reproduces the "metallicity effect". Dodson-Robinson et al. (2006) derived a fit for the time until gas runaway accretion is triggered by a planetary core at a fixed distance of 5.2 AU, as a function of the planetesimal surface density. They used this fit to estimate the frequency of giant planets as a function of several disk properties. We show our results regarding this subject in Sect. 8, where we compare it with their results. Matsuo et al. (2007) used parameterized formation models to determine the disk parameters where giant planet formation is possible either by core accretion or direct gravitational collapse. We present a similar study in Sect. 5.

The paper is organized as follows. Section 2 describes the methods used to obtain the result concerning the synthetic population presented in Sect. 3. Section 4 studies various aspects of the impact of disk properties on the mass of extrasolar planets, including the planetary initial mass function. Section 5 analyzes under which disk conditions giant planets can form. Section 6 addresses the correlations of disk properties with planetary migration and the final semimajor axis distribution. In Sect. 7 we study the metallicity of close-in planets. Section 8 shows how disk properties determine the fraction of stars with giant planets, while Sect. 9 asses the consequences if disk masses and lifetimes are correlated. Finally, in Sect. 10 we summarize the results and present our conclusions.

2. Methods

As our approach to planet formation and population synthesis was described in detail in Paper I, we limit here ourselves to a short overview.

2.1. General procedure

To obtain a synthetic population of planets, we proceed in five steps: (1) the probability distributions for the initial conditions are derived from observations of protoplanetary disks; (2) a large numbers of sets of initial conditions are drawn from these probability distributions according to the Monte Carlo method; (3) the corresponding final outcomes of the planet formation process (planetary mass and position) are computed using our planet formation model. This results in a population of synthetic planets, most of them however undetectable with current observational techniques; (4) to obtain the subset of the potentially observable synthetic planets, we apply an appropriate detection bias. Since most planets have been discovered by radial velocity techniques, we use a bias based on the velocity amplitude of the host star; (5) correlations between the initial (disk) conditions and the planetary properties are searched and compared to observations (if existing).

2.2. Initial conditions – probability distributions

We use four Monte Carlo variables to specify the initial conditions. (1) The dust-to-gas-ratio $f_{\rm D/G}$, which we link to [Fe/H] as [Fe/H] = $\log(f_{\rm D/G}/f_{\rm D/G,\odot})$, where $f_{\rm D/G,\odot}$ is the dust-to-gas ratio of the solar nebula for which we assume a value of 0.04. The choice of this value was discussed in detail in Paper I. Here we only briefly mention that the factor two to three by which 0.04 is greater than the measured photospheric Z of the Sun (Lodders 2003) is a first-order representation of the effects of dust evolution and drift. These mechanisms lead to an increase in the "planetesimal" $f_{\rm D/G}$ compared to the original "dust" $f_{\rm D/G}$ in the inner, planet-forming parts of the disk by a similar factor through the advection of material from the outer disk (Kornet et al. 2004). The probability of occurrence of a given [Fe/H] is derived from the metallicity distribution of the FGK stars in the CORALIE planet search sample (Udry et al. 2000), which is representative of the [Fe/H] distribution of the target stars in the various major radial velocity search campaigns (Paper I). Thus, we assume that the observed stellar metallicity is a good indicator of the primordial disk metallicity (Santos et al. 2003; but see also Pasquini 2007). (2) The initial gas surface density Σ_0 at $a_0 = 5.2$ AU, which we link to the initial disk gas mass $M_{\rm disk} = 4\pi\Sigma_0 a_0^{3/2}(\sqrt{a_{\rm max}} - \sqrt{a_{\rm min}})$. The probability distribution of circumstellar disk masses is derived from the observations of the ρ Ophiuchi star forming region (Beckwith & Sargent 1996). (3) The rate of photoevaporation $\dot{M}_{\rm w}$. The distribution of $\dot{M}_{\rm w}$ is constrained by the observed disk age distribution. We have adjusted our $\dot{M}_{\rm w}$ distribution to obtain, together with our value of the viscosity parameter α, a distribution of disk lifetimes $\tau_{\rm disk}$ that is in good agreement with the observed distribution (Haisch et al. 2001). (4) The initial semimajor axis of the planetary seed $a_{\rm start}$. The distribution of the starting positions of planetary embryos is not constrained by observations, and only theoretical arguments can be used. They indicate (e.g. Mordasini et al. 2009a) that runaway bodies should emerge with a uniform distribution in $\log(a_{\rm start})$, as already adopted by Ida & Lin (2004a).

In addition, we assume that these Monte Carlo variables are independent variables, so we do not consider any potential correlations arising during disk formation itself, e.g. via opacity effects. That we draw Σ_0 and $\dot{M}_{\rm w}$ independently implies, on average, a longer disk lifetime $\tau_{\rm disk}$ for more massive disks. The importance of this coupling is discussed in Sect. 9. We also do not consider here the influence of varying initial disk radii (Kornet et al. 2005). This will be considered in future work that will take recent observational results into account (Andrews et al. 2009, 2010).

2.3. Planet formation model

We use a slightly modified version (see Mordasini et al. 2009a) of the extended core accretion formation model described in detail in Alibert et al. (2005a). As in Pollack et al. (1996), we compute the evolution of the planetary core and envelope structure, but include disk evolution using the α formalism, and planetary migration (isothermal type I and type II). We were able to show (Alibert et al. 2005b) that the model reproduces many observational constraints imposed by our own giant planets.

2.3.1. Relevant model assumptions

For the disk-planet correlations discussed in this work, a number of model assumptions were found to be particularly relevant and to have directly visible consequences in the correlations. The first one concerns the structure of the protoplanetary disk, and specifically the location of the iceline. In the nominal model, the position of the ice line is an increasing function of disk mass due to viscous dissipation (Papers I and III; Min et al. 2011). It is found that this has important consequences on both the mass of giant planets (Sect. 4.3.1) and their formation location (Sect. 5.2.1).

A second assumption that is directly relevant for the masses of giant planets (Sects. 4.3.2 and 4.4) is that we assume that gap formation does not reduce the gas accretion rate of giant planets (Lubow et al. 1999). As explained in Paper I, this is because Kley & Dirksen (2006) have shown that, when a giant planet becomes sufficiently massive, the disk-planet system can undergo an eccentric instability. The planet then leaves the clean parts of the gap, resulting in a substantial increase in the gas accretion rate. This means that the gas accretion rate is obtained for low-mass planets ($M_{\rm core} \lesssim 10\ M_\oplus$) by solving the planetary structure equations, while for more massive planets in the disk-limited, runaway gas accretion phase, it is equal to the rate at which gas viscously flows towards the star in the disk $\dot{M}_{\rm enve} = \dot{M}_{\rm disk} = 3\pi\nu\Sigma$ where ν is the disk viscosity, and Σ the gas surface density.

A third setting that is relevant to the correlation of migration and metallicity (6.1.2) is that we assume that the planetesimal accretion rates are independent of the migration rate. The $\dot{M}_{\rm core}$ is calculated in the same way as in Pollack et al. (1996). Possible shepherding effects are not included for the reasons explained in Paper I. This means that cores in low solid-surface density disks still can grow relatively massive by migration.

Fourth, we assume for type II migration that as soon as the planet is more massive than the local disk mass ($M_{\rm planet} > \Sigma a^2$ where a is the semimajor axis), the migration rate is given as $-(3\nu/a) \times (\Sigma a^2/M_{\rm planet})^p$. In the nominal model, we use $p = 1$ ("fully suppressed" case, Armitage 2007). This is important for understanding the absence of a strong correlation of [Fe/H] and the semimajor axis (Sects. 6.1.1 and 6.3.3).

We simplify the problem significantly by assuming that only a single planet can form in a given disk. This would be correct in the limit that protoplanets can form within a single system without influencing each other. This is clearly an idealization, but in the context of this study, it is not necessarily a disadvantage. It allows one to see disk-planet correlations clearly, which otherwise might get partially blurred due to the random character of the (gravitational) interactions between several protoplanets.

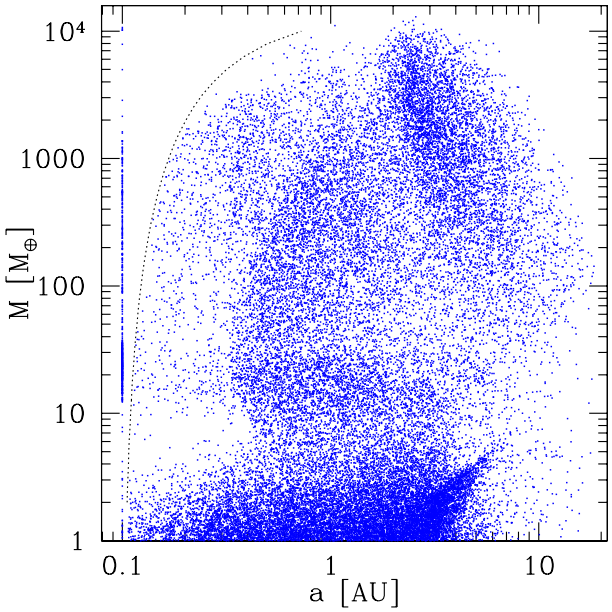

Fig. 1. Mass-distance diagram of the synthetic population analyzed in this work. The dashed curve shows the feeding limit (cf. Paper I): planets reaching this limit have been arbitrarily set to 0.1 AU.

Thommes et al. (2008) discuss extensively some of the effects induced by the concurrent formation of several planets in one disk.

The population discussed here is essentially obtained, except if otherwise mentioned, with identical parameters and Monte Carlo distributions as the nominal population presented in Papers I and II. In particular, this means that the stellar mass is equal to one solar mass $M_\odot$, the gas disk viscosity parameter α is 0.007, and the type I migration efficiency factor f_I is 0.001.

However, there is one relevant aspect in which the procedure used here differs from the one used in Papers I and II. We draw the initial semimajor axis of the starting seed strictly uniform in $\log(a_{\rm start})$ and disregard the additional criteria mentioned in Paper I. This eliminates some correlations present already in the initial conditions and thus makes it easier to identify the influence of disk properties on the planetary properties.

As a practical unit for the disk gas masses, we define, in analogy to [Fe/H], a relative logarithmic unit, denoted $[M_D/M_{SN}] = \log(\Sigma_0/\Sigma_{0,SN})$, where we assume an initial gas surface density at 5.2 AU $\Sigma_{0,SN} = 200$ g/cm^2. This is somewhat more than plain MMSN values – Hayashi's (1981) value would be about 145 g/cm^2 – but with this choice $[M_D/M_{SN}]$ covers, as for [Fe/H], a nearly symmetric range around zero between −0.6 and +0.7 for the values of Σ_0 considered here (50–1000 g/cm^2, corresponding to disk masses between about 0.004 and 0.09 $M_\odot$). As the disk gas mass M_D and the initial gas surface density Σ_0 are directly proportional to each other, these two terms are often used in an interchangeable way.

3. Mass-distance diagram

To provide an overview of the synthetic planet population we analyze in this work, we plot in Fig. 1 the mass-distance diagram of the entire population. In the figure, a number of structures already discussed in Paper I can be identified again, such as the low-mass "failed cores", the approximately Neptunian mass "horizontal branch", or the massive "outer group" planets outside a few AU. We also see that there are no very massive planets close-in. This is a consequence of the fact that planets with a higher mass than the local disk mass migrate at a reduced rate because their inertia is too much for the finite angular momentum flux in the disk. Their absence at small a depends upon the assumed degree of reduction of the type II migration rate once the planet is massive (Syer & Clarke 1995).

3.1. Paucity of low-mass, close-in planets

There is also a relative paucity of low mass ($4 \lesssim M \lesssim 10\ M_\oplus$) close-in ($a \lesssim 0.3$ AU) planets. Recent observations (e.g. Howard et al. 2010; Mayor et al. 2011) instead indicate a high frequency of low-mass super Earth planets close to their parent star.

Concerning this issue, we first recall that our model shows the state of (proto-)planets at the moment when the disk disappears, and not the final one after billions of years of evolution. At this stage, the low-mass protoplanets at small distances have a mass about equal to the local (solid) isolation mass (type I migration is strongly reduced in this simulation), which is on the order of 0.1 $M_\oplus$ only. Further growth from these masses to the final masses by giant impacts (e.g. Marcus et al. 2010) will then only occur after the damping influence of the gas disk is gone (Ida & Lin 2010), a phase which is however not included in our model at the moment. This effect would populate the depleted region from "below".

Second, the high observed frequency could be indicative of quite efficient type I migration, at least in some parts of the disk. This would populate the depleted region from "outside". Large quantities of low mass, close-in planets are found in some synthetic populations too, but only for high type I efficiency factors ($f_I \sim 0.1-1$) as shown in Fig. 11 of Paper II. On the other hand can the distribution of semimajor axes of giant planets at larger distances only be reproduced when the type I migration rate (as found from linear theories for isothermal disks) is reduced by a significant factor ($f_I \lesssim 0.01$, Paper II; Schlaufman et al. 2009). Here we are using the same low type I efficiency factor $f_I = 0.001$ which lead in Paper II to the best reproduction of the observed properties of giant planets. Unfortunately, this causes in the same time necessarily also the depleted region.

The answer to this dilemma is probably a significantly more complex migration pattern than what can be mimicked with global (independent of planet mass and distance) efficiency factors like f_I for isothermal type I rates as done here. Recent studies of type I migration dropping the often inappropriate assumption of isothermality (e.g. Paardekooper et al. 2010; Masset & Casoli 2010) indeed find complex patterns with rapid in- and outward migration. First exploratory planet population syntheses using such updated type I migration models (Mordasini et al. 2011b) find that type I migration is directed outward in some parts of the disk, and inward in others, which leads to the existence of convergence zones (migration traps), which can in turn result in a pile-up of many low-mass planets in certain parts of the disk (cf. Lyra et al. 2010; Sandor et al. 2011). This important subject will be addressed in a dedicated work (Dittkrist et al., in prep.).

A third mechanism occurs when several planets form and migrate concurrently. Then, lower mass planets can be pushed close to the star after being captured in mean motion resonances of a more massive, more rapidly migrating outer planet. This will be studied in future simulations that allow the formation of many planets per disk (Alibert et al., in prep.)

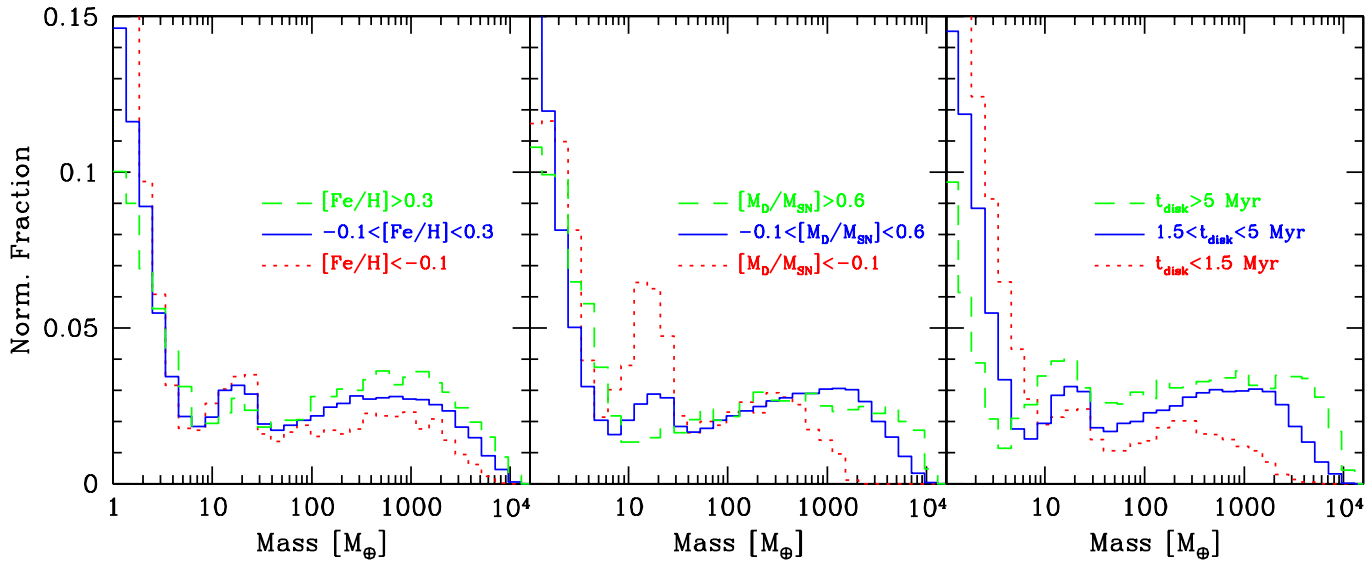

Fig. 2. Planetary initial mass function at the moment when the gaseous disk disappears. The models do not include any growth processes like giant impacts after disk dispersal, which can significantly modify the mass distribution afterwards, especially for low-mass planets with $M \lesssim 10\ M_\oplus$. *Left*: PIMF binned according to metallicity. *Center*: PIMF binned according to the gas disk mass. *Left*: PIMF binned according to the disk lifetime. The meaning of the different lines, and the limiting values, are indicated in the plot.

4. Mass

4.1. Planetary initial mass function (PIMF)

A central outcome of population synthesis is the planetary initial mass function PIMF (Papers II and III). Figure 2 shows the PIMF of all synthetic planets with a mass higher than 1 $M_\oplus$, binned into low, medium, and high metallicity (left panel), disk gas mass (central panel), and disk lifetime (right panel). The diving values are indicated in the plot and are chosen for all three cases in such a way that the central bin contains about 70% of the planets, and the other two about 15% each. We recall that our models start with an initial seed mass of 0.6 $M_\oplus$, so that we cannot reliably make predictions about the exact form of the PIMF in the $\lesssim$10 $M_\oplus$ domain as mentioned in Papers I and II. Each bin has been normalized individually, so that the absolute height of different bins (e.g. low vs. medium metallicity) cannot be compared in absolute terms, but only when taking into account that the initial distribution of [Fe/H] follows the distribution observed in the solar neighborhood. However, one can directly see the relative importance of a given planetary type within a bin (e.g. at high metallicity there are more Jovian than Neptunian planets, in contrast to the low [Fe/H] case). One again recognizes a number of features discussed in Paper I, like the high-mass tail in the super-Jupiter domain, the giant's plateau in the Jovian mass regime, the minimum at about 30–40 $M_\oplus$ corresponding to the planetary desert (Ida & Lin 2004a), the Neptunian bump and the strong rise towards low masses.

4.1.1. PIMF as function of metallicity

The left panel shows that the metallicity just modifies the importance of the three basic families of planets visible in the PIMF (Jovian planets, Neptunian planets, prototerrestrial planets), without however changing the general shape of the PIMF (in contrast to the other two disk properties). For giant planets, this means that in a high-metallicity environment, more giant planets form, but their mass distribution is similar. The reason for this is related to the fact that a certain [Fe/H] acts as a threshold for giant planet formation (threshold solid surface density to reach a critical core mass, see Sect. 5), but is not important in determining the final total mass, because in the end, gas makes up for most of the mass of a giant planet, and not solids. Therefore, high metallicity mainly allows a larger number of high-mass planets, but not of a higher mass (except for very high masses, see Sect. 4.3). This increase in frequency is of course the underlying reason for the observed metallicity effect, i.e. the increase in the detection rate of giant planets with [Fe/H] (see Sect. 8.1).

Moving down in mass, we see that in the Neptunian mass domain, the dependence of planet frequency on metallicity is weak. This means that no metallicity effect is predicted in this domain. This is in good agreement with recent observations (Mayor et al. 2011). Moving further down in mass to the prototerrestrial domain, the lines are inverted relative to the giant planet domain, which means that an inverse metallicity effect occurs (low-mass planets are more frequent at low [Fe/H] compared to high [Fe/H]). Concerning this last point, we must take into account that in our model, only one embryo can form per disk. The situation that, in high [Fe/H] disks, both a giant planet and a "byproduct" terrestrial planet form is therefore not possible. This could artificially strengthen the [Fe/H]-low mass planet anti-correlation, so that more secure predictions will be possible with models dropping the one-embryo-per-disk simplification (Alibert et al., in prep.). Observationally, future high-precision observations (e.g. with ESPRESSO) will test this prediction.

One further notes that for all three bins, the highest peak in the mass function is found for the prototerrestrial planets, with the clearest dominance at low metallicity. For high metallicity, the second highest peak occurs for the giant planets, whereas for intermediate and, even more clearly, for low metallicity, the Neptunian planets are responsible for the second highest peak.

4.1.2. PIMF as function of disk gas mass

The central panel shows that the disk mass distribution directly affects the shape of the PIMF and not only the height of the peaks of the distribution as metallicity does. For giant planets,

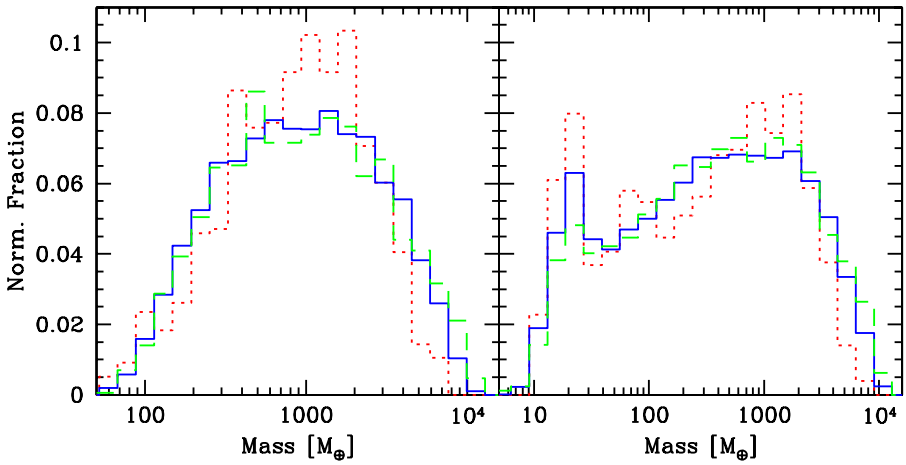

Fig. 3. Planetary mass function binned according to [Fe/H] as in Fig. 2, left panel, but now only for the subpopulation of potentially detectable synthetic planets with an RV precision of 10 m/s (*left panel*) and 1 m/s (*right panel*). Green dashed lines again represent high, blue solid lines medium and red dotted lines low metallicities, where the threshold metallicities are the same as in Fig. 2.

a high $[M_{\rm D}/M_{\rm SN}]$ shifts the formation of giant planets from lower mass to higher masses (compare the blue and green lines). For lower disk masses, massive giant planets ($\gtrsim 6\,M_{\rm J}$) cannot form at all. In this case, there is simply not enough gaseous material available. The distribution of intermediate-mass planets ($30\,M_\oplus \lesssim M \lesssim 1\,M_{\rm J}$), on the other hand, is barely affected. We conclude that there is a direct correlation in our model between the (maximum) mass of giant planets and the disk gas masses. This is essentially because giant planets accrete most of their mass in a regime where their accretion rate is proportional to the disk mass (see discussion in Sect. 4.4).

In Paper III, we showed that, in our alpha-disk model, the disk mass has to be scaled roughly linearly with M_* in order to reproduce the observed correlation between the star's accretion rate and its mass. As shown in this paper, this translated into the formation of planets of a higher mass orbiting stars of a higher mass, in good agreement with observations (Lovis & Mayor 2007). Even though we did not vary the stellar mass in the present study, that more massive planets form in disks taken from the high-mass end of the distribution stems from the same reason. Unfortunately, in practice we cannot infer the primordial disk mass for any actually detected exoplanet, so this correlation is difficult to test observationally in contrast to the metallicity correlation. The panel further shows that the relative importance of Neptune-like planets strongly depends on the disk's gas mass. Neptune-like planets form particularly easily in disks with low primordial disk masses, while they do not seem to be able to form in massive disks. This again is a consequence of the same effect discussed above and already pointed out in Paper III.

4.1.3. PIMF as function of disk lifetime

The third panel at the right of Fig. 2 finally shows the disk lifetime. The disk lifetime has a twofold influence. In disks with longer lifetimes, cores will be able to grow to the critical mass and accrete gas in a runaway fashion even for a relatively low solid surface density. Therefore, the disk lifetime acts as a threshold for giant planet formation, similar to the metallicity. The lifetime of disks, however, also affects the total mass of the planets similar to the disk mass, as, to first order, the planet's final mass will be equal to the accretion rate times the duration of the accretion phase. This twofold effect is clearly seen in the figure. Giant planets formed in long-lived disks are both numerous and have a higher mass. Compared to metallicity and disk masses, the disk lifetimes thus have a more complex influence on the resulting planet population. The disk lifetime both scales and distorts the shape of the PIMF. Similar to the primordial disk mass, it is difficult to deduce the disk lifetime for any give observed system. We come back to that in Sect. 8.

4.2. Observable distribution as function of [Fe/H]

It is interesting to look whether some of the correlations between disk properties and the underlying mass function (of all planets) discussed in the section above can already be seen in the observational data we have today, which represent only a small fraction of all existing planets. For this, we plot the mass histogram binned according to [Fe/H] in Fig. 3, but now including only planets detectable by a ten-year duration radial velocity (RV) survey with a precision of either 10 m/s (left panel) or 1 m/s precision (right panel). As in Paper III, we use a very simple velocity amplitude cut-off criterium to determine detectability.

4.2.1. 10 m/s radial velocity precision

The figure shows that at a precision of 10 m/s, the mass distribution has a very similar shape for all three metallicity bins, as expected from the discussion above and the previous work by Ida & Lin (2004b). However, a closer look indicates that the low [Fe/H] bin has a somewhat narrower distribution and that there is a certain systematic difference at the upper mass end (see the next section). However, the medium and high-metallicity bins, to which most of the currently known planet population belongs, are very similar. It is therefore not surprising that, given the relatively small number of observed planets compared to the large number of synthetic planets used here, no significant correlation between the shape of the mass distribution of giant planets and the host star metallicity has been noticed thus far.

4.2.2. One m/s radial velocity precision

At a precision of 1 m/s, in contrast, the influence of [Fe/H] on the PIMF becomes visible as measured by the relative frequency of Neptunian versus Jovian planets, a trend that has been observed by Udry et al. (2006). We find that the ratio of the number of Neptune-mass to Jupiter-mass planets strongly correlates with the metallicity. For the low metallicity, the Neptune-mass planets are almost as numerous as Jupiter-mass planets, while they are significantly less frequent for high-metallicity disks. This corresponds well with the observed result (Sousa et al. 2008). The numerical values of the ratios of synthetic Jupiter-to-Neptune number of planets (dividing mass defined at $30\,M_\oplus$) obtained for

a ten-year search at 1 m/s is in our nominal simulation 4.7, 5.8, and 7.6 for the low, medium and high [Fe/H] bins, respectively. These values are difficult to directly compare with Sousa et al. (2008) because of the difference in metallicity bins, primary masses, and survey duration. However, these authors find values for the Jupiter-to-Neptune ratio of 1.6–5 for [Fe/H] < −0.15, and 7.5–30 for [Fe/H] > 0.15. The ratios even at 1 m/s precision are higher than those in the full underlying distribution with no detection bias. The reason is that even at 1 m/s many Neptune-like planets remain undetected. Finally, we point out that our one-planet-per-disk simplification makes it very likely that our ratio is an upper limit. A hint in the same direction can also be inferred when comparing our synthetic result with the observed one shown in Fig. 10 of Mayor et al. (2011). Otherwise, observed and synthetic results are similar.

From the two plots we also understand that the decrease in the observed mass distribution at 10 m/s towards low masses, while clearly being the consequence of the observational detection bias against low-mass planets, is amplified by the actual true decrease in the underlying mass distribution. This degree of depletion of intermediate-mass planets (30−100 $M_\oplus$) is potentially an important constraint on the gas accretion rate at the beginning of runaway gas accretion. In Mordasini et al. (2011a), we presented a detailed discussion about various assumptions about gas accretion that directly determine this portion of the theoretical PIMF.

4.3. (Maximal) planetary masses and metallicity

To emphasize the importance of the metallicity (measured in our model by the ratio of dust-to-gas in the disk) on the resulting high end of planetary masses, we show in Fig. 4 the mass of synthetic planets (in units of Jupiter masses) as a function of metallicity. While we have indicated in Sect. 4.1 that metallicity does not significantly change the distribution of the mass for the bulk of the population, we see here that the metallicity determines the maximum mass a planet[1] can grow to in a given disk, in particular for subsolar metallicities. There is an absence of very massive planets around low-metallicity stars. This can be understood as follows. To grow to a very high mass, a critical core must form before viscous evolution and photoevaporation of the disk have had time to significantly deplete the disk mass. Such a very early start is not possible in a low-metallicity environment where growing large cores take longer.

This second-order correlation via the core formation timescale has been checked and confirmed by artificially reducing the starting time of the seed embryos by a factor of two. In this test, the maximum mass of planets at [Fe/H] = −0.4 increases to about 18 $M_\oplus$ compared to ∼7 $M_\oplus$ in the nominal case.

4.3.1. Effect caused by the iceline position

A less pronounced absence of massive planets at low metallicity can also be obtained if we fix the position of the ice line at 2.7 AU independently of the disk gas mass, as expected for an optically thin disk irradiated from a 1 $M_\odot$ star (Ida & Lin 2004a). This difference is due to an interesting chain of correlations:

1) we recall that in the nominal case, the position of the ice line is an increasing function of disk mass;
2) at low metallicities, high disk gas masses are needed for giant planet formation (Matsuo et al. 2007; Sect. 5.3). Thus, the ice line position in low-metallicity disks forming giant planets will typically be located at large distances;
3) as a result, the typical starting position of giant planets-to-be will also be at a large distance at low metallicities ($a_{\rm start} \gtrsim a_{\rm ice}$, see Sect. 5.2);
4) this distant starting position implies slower growth of the core (e.g. Paper I), which is disadvantageous for successful giant planet formation.

Thus, a positive correlation of the disk gas mass and the iceline position renders giant planet formation at low [Fe/H] even more difficult, and makes it impossible to populate the upper left-hand corner of Fig. 4 with the nominal model. It also means that there is a difference between a metal poor-gas rich and a metal rich-gas poor environment, even if the solid surface density beyond the ice line are in principle the same. A low [Fe/H] cannot in all circumstances be compensated for by a high disk gas mass.

In the case with an ice line independent of $[M_{\rm D}/M_{\rm SN}]$, this complex chain of correlations between [Fe/H], $[M_{\rm D}/M_{\rm SN}]$, $a_{\rm ice}$, $a_{\rm start}$ and $t_{\rm start}$ is broken, and planets with about 10 $M_\oplus$ can still form at [Fe/H] = −0.5. Maximum masses already become independent of [Fe/H] for [Fe/H] ≳ −0.3. The upper limit of possible masses is indicated for this case in Fig. 4. It is clear that this chain of correlations is quite sensitive to a number of specific model assumptions, making it a less robust prediction.

4.3.2. Very massive planets

The absence of very massive companions formed by core accretion at very low metallicities is also seen in the models of

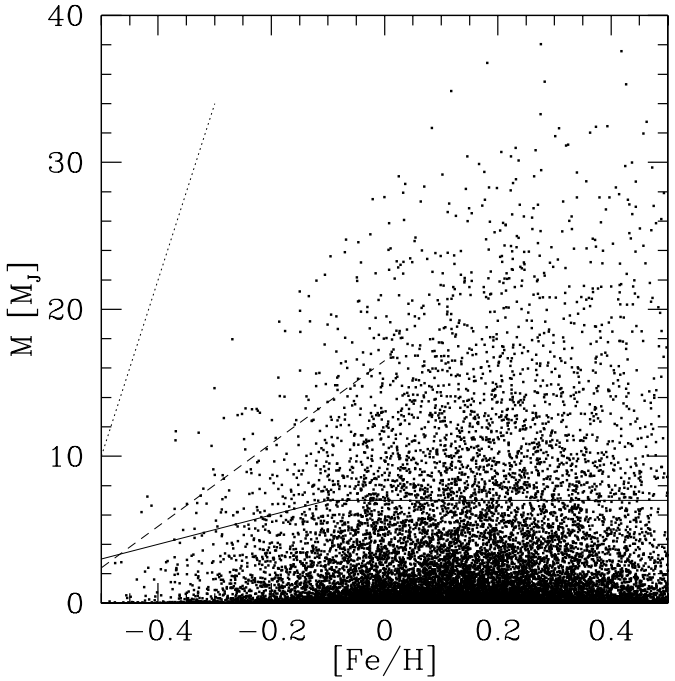

Fig. 4. The mass of synthetic planets (in Jupiter masses $M_{\rm J}$) as a function of metallicity for the nominal population (small dots). In the plot, lines indicate approximatively the region of high mass and low metallicity where no synthetic giant planets are found in other non-nominal populations: with an ice line fixed to 2.7 AU (dotted line), or with the effect of gap formation on the gas accretion rate modeled as in Veras & Armitage (2004) (solid line). The dashed line shows the limit given in Fischer & Valenti (2005).

[1] We here call for simplicity all objects that form in the population synthesis planets, even if their mass is higher than the deuterium-burning limit at about 13 $M_\oplus$.

Ida & Lin (2004b) and Matsuo et al. (2007). However, compared to these works, planets of significantly higher mass can form in our simulations. This is a direct consequence of our assumption that gap formation does not reduce the gas accretion rate, as mentioned in Sect. 2.3.1. If instead in a non-nominal population we limit the gas accretion rate of giant planets due to gap formation using the fit of Veras & Armitage (2004), the maximum mass of all planets in the population is reduced to $\sim 7\ M_\oplus$. The absence of the most massive objects at low metallicities remains similar, but with a weaker dependence of the maximum mass on metallicity when scaled to lower absolute masses. The approximative limiting envelope for such a population is also shown in Fig. 4 as a solid line. This envelope is now similar to the one of Matsuo et al. (2007). We thus see that, while the tendency towards the absence of very massive planets at low metallicities is a general prediction of the core accretion theory, the quantitative results depend on specific model settings.

When studying the figure one should keep in mind that very massive planets ($\gtrsim 10 M_\oplus$) are in fact very rare outcomes in our simulations, in agreement with the observed "brown dwarf desert" discussed in Paper II. Figure 4 may provide the somewhat misleading impression that these are common objects, while in fact they only appear numerous because the underlying synthetic population is extremely large (about 200 000 initial conditions). Even if such a population vastly exceeds the actually observed population, these high numbers of planets are required to investigate the different correlations, some depending on two variables (such as disk mass and [Fe/H]).

4.3.3. Comparison with observations

The absence of very high-mass planets (or of a very high total mass locked up in planets in multi-planet systems) at low metallicities has also been noted observationally in Udry et al. (2002), Santos et al. (2003), and Fischer & Valenti (2005). It is clear that such an absence could also simply be a small number effect: Giant planets around low-metallicity hosts are rare, and high-mass giant planets ($\gtrsim 5\ M_\oplus$) are rare at all metallicities, which could combine to create the observed paucity. It is interesting to compare our results with the observational database, especially since this base has been significantly extended since those papers were published.

Such a comparison is presented in Fig. 5, which shows the masses of actual and synthetic planets as a function of metallicity. Observational data was taken from J. Schneider's Extrasolar Planet Encyclopedia. This database does not include companions larger than about 20 $M_\oplus$. However, such companions are anyway extremely rare, both in the model (only 0.1% of the synthetic planets have a mass higher than 20 $M_\oplus$) and in observations. As a result, our observational knowledge of this mass range, where several formation mechanism could contribute, still suffers from small number statistics (see also Sozzetti & Desidera 2010).

In Fig. 5, planets detected by the radial velocity method around primaries with a mass between 0.8 and 1.2 $M_\odot$ are the most relevant cases (in the model $M_* = 1\ M_\odot$) but we also show companions to stars more massive than this, also detected by radial velocity. Stars which have evolved off the main sequence (if known) are marked in the figure. Stellar evolution could be of relevance here, as it might invalidate our underlying assumption that the photospheric composition measured today correlates with the bulk composition of the disk material at formation. This assumption could be invalid in case of enhanced heavy element settling, which for the Sun seems to have already lead to a reduction of the present-day Z as compared to the primordial Z_0 by more than 10% (Lodders 2003).

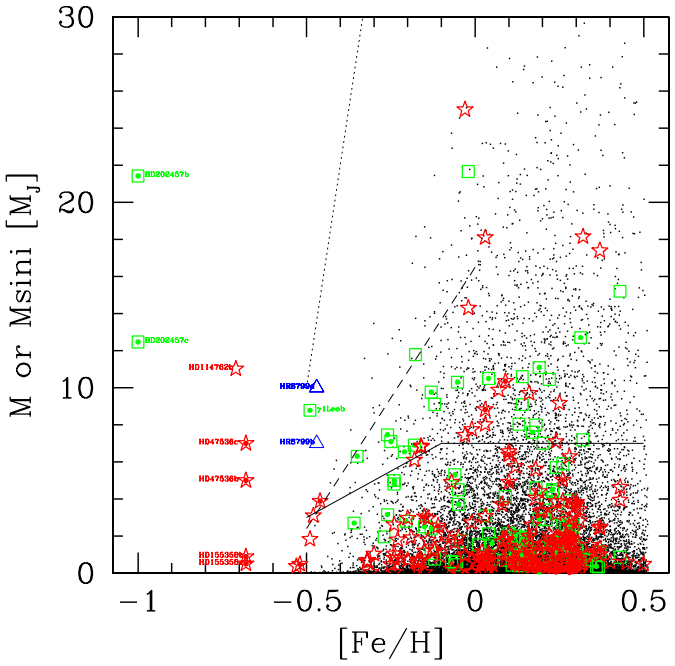

Fig. 5. Observed and synthetic planetary masses as a function of metallicity. Black dots denote synthetic planets in the nominal model, while solid, dashed, and dotted lines again indicate the limiting envelope of non-nominal models, as in Fig. 4. Red stars are observed RV companions around stars with $0.8 < M_*/M_\odot < 1.2$. Green squares are observed RV planets around stars with a mass higher than 1.2 $M_\odot$. For both cases, a point in the middle of the symbol indicates that the star is a subgiant or giant. Blue triangles show planets around HR 8799. Names of relevant objects are given in the plot.

Looking at Fig. 5, we see that the bulk of all observationally detected planets falls into regions of the plot where synthetic planets are also found. From this observation we could thus conclude that core accretion can account for almost all planets that are currently known. This conclusion has already been reached by Matsuo et al. (2007). It should be noted that surveys that look at very metal-poor stars do exist (Santos et al. 2009).

4.3.4. Relevant individual objects

However, eight RV planets orbiting five stars clearly lie outside the region where giant planets form orbiting a 1 $M_\odot$ star in our nominal model. This group is characterized by a much higher fraction of giant stars and of stars more massive than 1.2 M_* than found in the full sample. It also has a high multiplicity for giant planets. Since some of the objects are quite peculiar, it is worth discussing some of these objects individually.

HD 155358 has two planetary companions of rather low mass ($\lesssim 1\ M_\oplus$) at 0.6 and 1.2 AU (Cochran et al. 2007). It has a mass of $0.87 \pm 0.07\ M_\odot$ and [Fe/H] = -0.68 ± 0.07. HD 155358 is a particular star (Fuhrmann & Bernkopf 2008), because it is a very old, thick disk subgiant with a chemical composition very far from scaled solar composition. It is significantly enriched in alpha-chain nuclei. [Mg/H] is, for example, with −0.36 much higher than [Fe/H]. What matters for the ability to form a sufficiently massive core is the surface density of all condensible elements beyond the ice line, which can attribute important quantities of matter, in particular the α elements O, Si, and Mg (Dodson-Robinson et al. 2006; Gonzalez 2009). Due to the

enrichment in α elements, the disk around HD 155358 was depleted in planetesimals maybe only by a factor 2 below a solar composition disk with [Fe/H] = 0, equivalent to [Fe/H] ~ -0.3 if it were to have a scaled solar composition. At such a value, forming the low-mass giant planets is certainly possible with the core accretion mechanism.

HD 114762, with its $M \sin i = 11\,M_\downarrow$, $a = 0.36$ AU companion (Latham et al. 1989) has been already discussed in this context by Udry et al. (2002). It has been often considered that the system is seen nearly pole on, so that the companion might in fact be a late M dwarf (Cochran et al. 1991; Hale 1995). An alternative hypothesis is based on the finding that HD 114762 is chemically and evolutionary very similar to HD 155358 (Fuhrmann & Bernkopf 2008), which would mean that its effective surface density of planetesimals was much higher than one would infer from the low iron content and scaled solar composition.

HD 47536 is an old K1III, [Fe/H] = −0.68 giant, which is orbited by one (Setiawan et al. 2003), possibly two (Setiawan et al. 2008) quite massive companions (5 and 7 $M_\downarrow$) inside a few AU. While Setiawan et al. (2003) originally quoted a possible stellar mass of about 1 to 3 $M_\odot$, da Silva et al. (2006) more recently determined a mass of $0.94 \pm 0.08\,M_*$. With this primary mass, the object falls clearly out of the envelope of synthetic planets in our model. In particular, if its two-planet configuration is confirmed, this is an interesting object to study with formation models, as one then cannot invoke a nearly pole-on orientation. Also for the direct collapse model this case is probably not obvious to explain owing to the small semimajor axis of the planets (about 1.5 AU for the inner planet), see e.g. Boley (2009).

BD+20 2457 is a K2II giant, with an estimated mass of $2.8 \pm 1.5\,M_\odot$, a very low metallicity of $[\mathrm{Fe/H}] = -1.00 \pm 0.07$, and two very massive companions in tight orbits (Niedzielski et al. 2009). Even if the very different primary mass makes a comparison with the results here difficult, these companions seem to be far from the possible parameter space for core accretion.

The object around γ^1 Leo A (HIP 50583) was found to have a projected mass of about 8.8 $M_\downarrow$ (Han et al. 2010). The orbit of the companion has, however, recently been astrometrically detected by Reffert & Quirrenbach (2011) in the *Hipparcos* data. Their results indicate a clearly higher actual mass of about 66 $M_\downarrow$ (with substantial incertitude). This moves the companion out of the relevant mass domain.

The plot also includes HR 8799 with a measured [Fe/H] = −0.47 (which might, however, not reflect the initial metallicity, Marois et al. 2008) and planets detected by direct imaging i.e. at large orbital distances (Marois et al. 2008, 2010). HR 8799 also probably has a mass over 1.2 $M_\odot$ ($1.5 \pm 0.3\,M_\odot$), so the synthetic population does not apply directly, but it is nevertheless interesting to note that these planets come to lie in a region in the [Fe/H]-mass plane, which is at or close to the limit where giant planets can originate from core accretion. This is a finding independent from the fact that the large semimajor axes of these planets makes core accretion as the formation mechanism difficult (Dodson-Robinson et al. 2009), if no additional mechanism causing outward displacement like scattering is acting.

4.3.5. Summary concerning the [Fe/H]-M correlation

In summary we see that there are only extremely few examples of bona fide, massive companions ($5 \lesssim M \lesssim 20\,M_\downarrow$) orbiting solar-like, main sequence stars at small orbital distances that do not fall into the [Fe/H]-M parameter space covered by our implementation of the core accretion model.

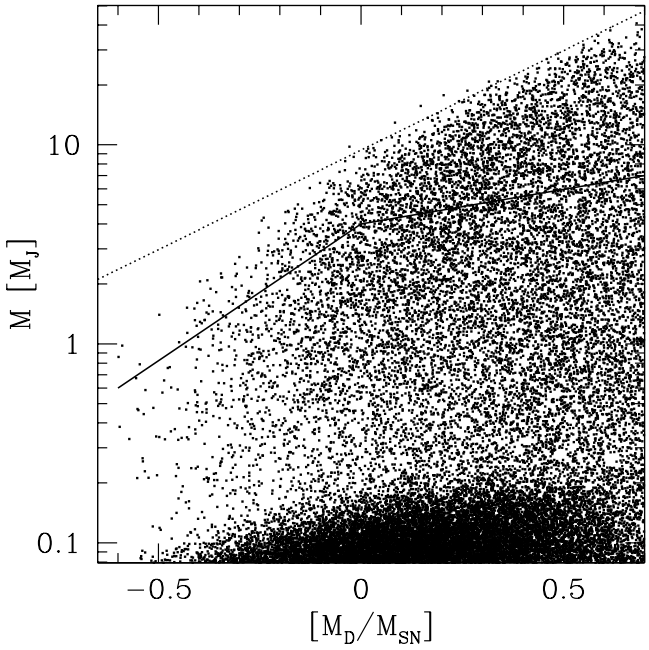

Fig. 6. The mass of synthetic planets (in Jupiter masses) as a function of the initial disk mass for the nominal population (black dots). The dotted line indicates a mass half as high as the initial gas disk mass, showing the linear correlation of disk mass and maximum planet mass for most of the domain. The solid line shows the upper limiting envelope in a non-nominal population where the limiting effect of gap formation on the gas accretion rate is taken into account, using the fit of Veras & Armitage (2004).

Figure 5 also shows the limiting envelope of synthetic planetary masses derived in the case where the gas accretion rate due to gap formation is limited by using the simple one parameter fit of Veras & Armitage (2004) to hydrodynamical simulations of Lubow et al. (1999). It is clear that such a simple fit can only be a rough approximation of the real effect and that, e.g., disk viscosity also influences the degree of quenching of gas accretion (Lissauer et al. 2009). But the significant number of planets lying above the solid line indicates that mechanisms like the eccentric instability (Kley & Dirksen 2006) that allow growth beyond the gap barrier seem to play an important role in nature.

We finally note that the most massive synthetic planets could also, at least partially, be an artifact of the one embryo per disk approximation. In a disk where several protoplanets grow concurrently, planets compete for gas and ejection can even remove some planets (Thommes et al. 2008). In this sense, looking at the total mass in the system should be a more adequate quantity than individual planet masses.

4.4. Planetary masses and disk mass

Figure 6 shows planetary masses as a function of the initial disk gas mass, again in units of Jupiter masses to focus on the massive planets. Here we find a different behavior than for the metallicity: As expected from the discussion of the influence of the disk gas mass on the PIMF, we see that there is a positive correlation of disk mass and planetary mass over the full domain of disk masses considered here. The plot illustrates that there is, for the domain of $[M_\mathrm{D}/M_\mathrm{SN}] \gtrsim -0.2$ an approximatively linear correlation between the maximum planet mass and the disk mass. The reason for this is that giant planets in our model (see Mordasini et al. 2009a) accrete most of their mass in the disk-limited

accretion regime where the planetary gas accretion rate is assumed to be the same as in the disk ($\dot{M}_{\rm env} = \dot{M}_{\rm disk} = 3\pi\nu\Sigma$), which is itself proportional to the initial disk mass for a given distance and moment in time, at least if the disk evolution is close to self-similarity solutions (Hartmann et al. 1998).

The different influence of [Fe/H] and disk gas masses on the mass of giant planets can be quantified. For planets with a mass higher than 100 $M_\oplus$, one finds that the median planetary mass grows for an increase in [Fe/H] from −0.45 to 0.45 only by about a factor 1.5 (from 512 to 747 $M_\oplus$). For an increase over the same $[M_{\rm D}/M_{\rm SN}]$ domain, in contrast, the median giant planet mass increases from 182 to 814 $M_\oplus$ i.e. by about a factor 4.5.

For $[M_{\rm D}/M_{\rm SN}] \lesssim -0.2$, the maximum masses decrease faster than linearly with decreasing $[M_{\rm D}/M_{\rm SN}]$ because at such low disk masses, the low resulting solid surface $\Sigma_{\rm S} = f_{\rm D/G}\Sigma_0$ densities becomes important in a second-order effect. The final planetary mass is no longer determined just by the amount of gas that can be accreted, but also by the time needed to form a supercritical core. This is an effect that is analogous to the dependence of the maximum mass seen at low metallicities. The exact value of the highest efficiency of converting disk gas into planetary envelope material (here about 0.5) depends on the exact treatment of the back reaction of the planet's accretion on the disk, but is found to lie in a domain of 0.3 to 0.5. The linear correlation between disk mass and maximum planetary mass is, however, not affected by different treatments. This indicates that a positive correlation of disk mass and giant planet mass is a stable prediction of the core accretion theory, while the quantitative degree depends on the model. For the large majority of giant planets ($M \geq 1\,M_\oplus$), the efficiency of converting disk gas into planetary material is lower (∼0.1), but with a very wide spread of possible values, depending on, e.g., the photoevaporation rate, the metallicity, or the disk gas mass itself.

Figure 6 indicates also the approximative upper envelope obtained for the non-nominal population using gas accretion rates limited by gap formation according to the Veras & Armitage (2004) fit. In this case, the planetary gas accretion rate is still proportional to $\dot{M}_{\rm disk}$ but decreases exponentially as $\exp(-M_{\rm planet}/1.5\,M_\oplus)$ with planet mass until a floor value of $\dot{M}_{\rm env} = 0.04\,\dot{M}_{\rm disk}$ is hit. The consequence is, as shown by the figure, that the clear correlation of disk mass and planet mass is now broken, as expected from the functional form of the equation. One finds that the maximum mass now depends only weakly on the disk mass, approximatively as $(M_{\rm D}/M_{\rm SN})^{1/4}$ for $M_{\rm D} \gtrsim M_{\rm SN}$. A weak correlation remains because of the floor accretion rate. At lower disk masses, the correlation is somewhat stronger, for the same reason as for the nominal population.

That maximum masses are linearly proportional to disk masses for the nominal population is interesting because one expects to see an imprint of the disk gas mass distribution on the planetary mass distribution. This is reminiscent of the situation for stars, where the protostellar core mass function CMF has a remarkably similar functional form to the stellar IMF (e.g. McKee & Ostriker 2007). This question will be addressed further in forthcoming work.

5. Disk conditions leading to giant planet formation

5.1. Minimal solid surface density

With the population synthesis calculations, one can study a posteriori which combinations of disk properties allow the formation of giant planets and, in particular, which are the most extreme ones. Comparable studies have been done in Kornet et al. (2006), Dodson-Robinson et al. (2006), Ikoma et al. (2000), or Thommes et al. (2008).

Figure 7 shows the relative planetesimal surface density $\Sigma_{\rm S}/\Sigma_{\rm S,SN}$ at 5.2 AU, where $\Sigma_{\rm S} = f_{\rm D/G}\Sigma_0$ is the planetesimal surface density in a given disk and $\Sigma_{\rm S,SN} = f_{\rm D/G,\odot}\Sigma_{0,\rm SN} = 8$ g/cm^2 is the planetesimal surface density in our solar nebula reference disk, which leads to the formation of a giant planet ($M \geq 300\,M_\oplus$), as a function of the starting position of the seed embryo. The core accretion rate $\dot{M}_{\rm core} \propto \Sigma_{\rm S}$ (e.g. Alibert et al. 2005a), therefore this quantity is a central control parameter within the core accretion formation paradigm. A value of e.g. $\Sigma_{\rm S}/\Sigma_{\rm S,SN} = 3$ thus corresponds to a disk with roughly three times more solids than the amount we assume for the solar nebula. In all disks, the solid surface density scales as $a^{-1.5}$ with a jump of a factor 4 at the ice line, therefore this value corresponds for a starting position of the embryo of e.g. $a_{\rm start} = 10$ AU (which is outside the ice line for all Σ_0 considered here) to a local planetesimal surface density at $a_{\rm start}$ of about $3 \times 8 \times (10/5.2)^{-1.5} = 9$ g/cm^2.

5.1.1. Preferred location for giant planet formation

The plot shows that the sweet spot for giant planet formation (i.e. the lowest solid surface densities that allow it) occurs at about 5 AU, at a value of about 0.75, corresponding to 6 g/cm^2. This value is similar to the result of Dodson-Robinson et al. (2006), who find that a solid surface density of about 6.5 g/cm^2 (also at 5.2 AU) is needed to bring an embryo to runaway gas accretion in 7 Myr, which corresponds to the longest living disks in our population (Paper I). At a starting position of 1 AU (inside the ice line), a $\Sigma_{\rm S}/\Sigma_{\rm S,SN}$ of at least 10 is needed, corresponding to a local planetesimal surface density of about $0.25\times10\times8\times(1/5.2)^{-1.5} \approx 240$ g/cm^2, which is in good agreement with Kornet et al. (2006). We see that at both smaller and larger distances, more massive disks of planetesimals are needed. This agrees with the works mentioned earlier. The abrupt increase by about a factor 4 at about 3–4 AU simply corresponds to the increase needed to compensate for the decrease in the planetesimal surface density inside of the ice line by an identical factor due to the sublimation of ices. The upper limit of $\Sigma_{\rm S}/\Sigma_{\rm S,SN}$ in the plot corresponds to disks where both $f_{\rm D/G}$ and Σ_0 come from the upper ends of their distributions.

5.1.2. Isolation mass and timescale effect

The reasons for the remaining increase in the necessary $\Sigma_{\rm S}$ with both increasing and decreasing $a_{\rm start}$, i.e., the existence of the sweet spot has been discussed in earlier work (e.g. Kornet et al. 2006; Thommes et al. 2008). Therefore we here only briefly illustrate this by the following two non-nominal populations which are also plotted in Fig. 7:

– The top right panel shows a population with a faster type I migration rate ($f_{\rm I} = 0.1$ instead of 0.001). In this case, the minimal necessary planetesimal disk mass is reduced at short distances. This shows that at short distances (where the core accretion timescales are small) the low isolation masses (and the associated long Kelvin-Helmholtz timescales for gas accretion) limit giant planet growth. Isolation masses decrease with decreasing semimajor axis, which must be compensated for by an increasing $\Sigma_{\rm S}$. Faster type I migration partially neutralizes this need, as it allows growth beyond the isolation mass and up to the critical mass by increasing the embryo's feeding zone (Alibert et al. 2004).

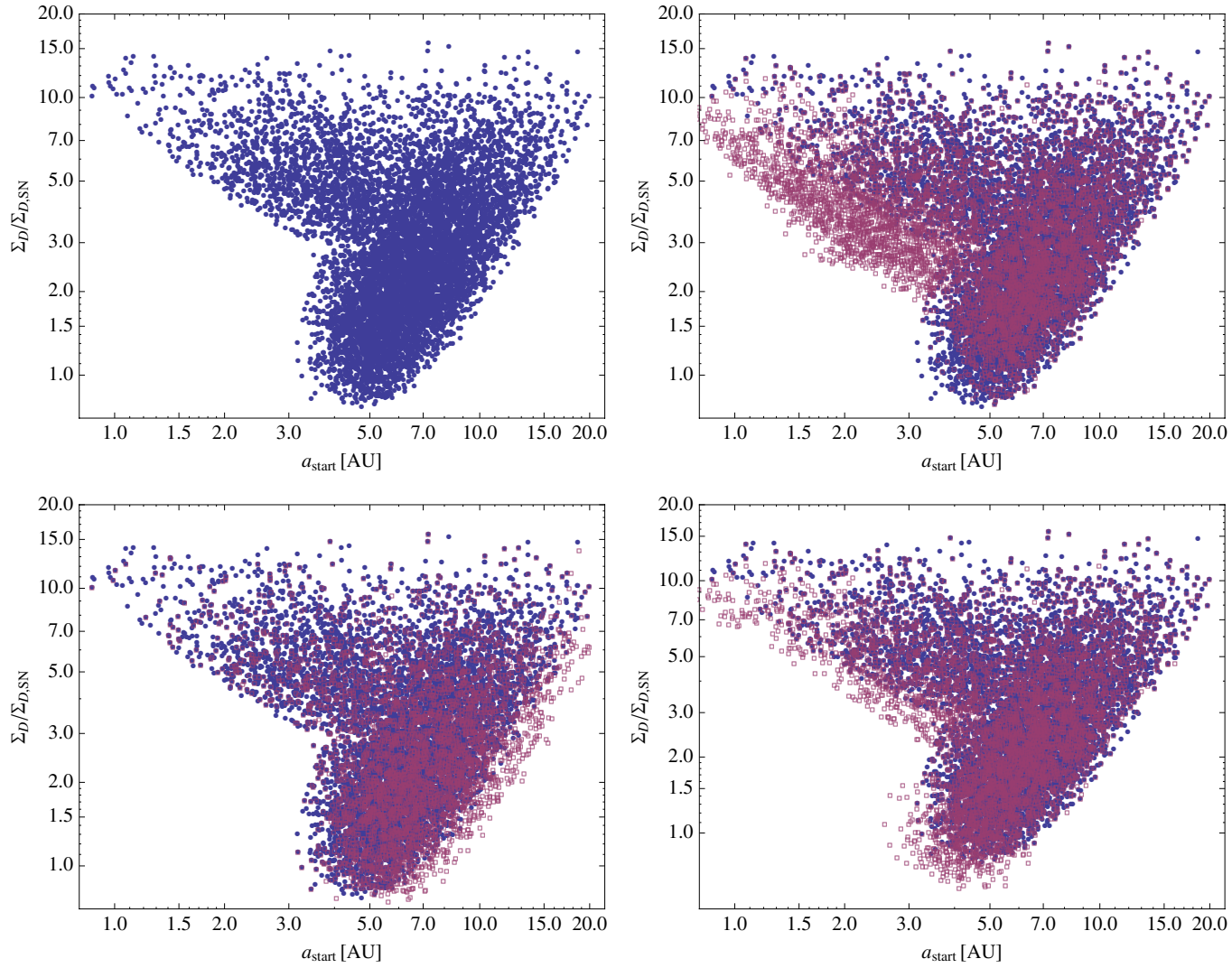

Fig. 7. Relative planetesimal surface density $\Sigma_S/\Sigma_{S,SN} = f_{D/G}\Sigma_0/(f_{D/G,\odot}\Sigma_{0,SN})$ at 5.2 AU leading to the formation of a planet with a final mass $M \geq 300\,M_\oplus$, as function of the starting position of the embryo a_{start}. A value of $\Sigma_S/\Sigma_{S,SN} = 1$ corresponds to an initial planetesimal surface density of 8 g/cm^2 at $a_0 = 5.2$ AU, while a value of, e.g., 3 corresponds at, e.g., 10 AU to 9 g/cm^2. The *top left panel* shows the nominal population only (blue dots). The three other panels show non-nominal population as open red squares that overlay the nominal population that is also shown for comparison, still with blue dots. *Top right*: population with faster type I migration ($f_I = 0.1$). *Bottom left*: population where t_{start} is reduced by 50%. *Bottom right*: population where the opacity in the planetary envelope is 2% of the interstellar value.

– The bottom left panel shows a population for which we have arbitrarily reduced t_{start} by a factor 2. In this case at large distances a difference is seen, while the points lie on top of each other in the other parts of the plot. At large distances, many solids are available in the embryo's feeding zone, but the core-growth timescale is very long. To compensate for that, i.e. to still build up a critical core during the disk lifetime, Σ_S must also increase towards the exterior. When we (artificially) speed up the accretion rate (or, equivalently, reduce t_{start}), this requirement is relaxed.

5.1.3. Situation of the solar nebula

The figure also shows that the solar nebula is not far above the overall minimal necessary Σ_S for giant planet formation. This conclusion also agrees with Thommes et al. (2008). We find that the overall minimal value is about $\Sigma_S/\Sigma_{S,SN} = 0.75$, i.e., $\Sigma_S \approx 6$ g/cm^2. This would correspond to an isolation mass at 5.2 AU of about 5.3 $M_\oplus$. Studying the total mass of accreted planetesimals (which can be in the core or dissolved in the envelope), we, however, find that the smallest mass of heavy elements in planets more massive than 300 $M_\oplus$ is clearly greater, namely about 23 $M_\oplus$. This is a consequence of migration and of planetesimal accretion also after runaway gas accretion is triggered. Internal structure modeling of observed transiting extrasolar planets by Miller & Fortney (2011) points to a similar minimal heavy element content of giant planets.

5.1.4. Impact of the grain opacity

The bottom right panel of Fig. 7 finally shows a population calculated with an opacity of 0.02 times the nominal (interstellar) value in the envelope (e.g. Pollack et al. 1996). Here we find that the minimal necessary value is, as expected, lower, about 4.7 g/cm^2. This reduction is rather small compared to the large effect of the opacity in formation calculations without migration (Pollack et al. 1996; Movshovitz et al. 2010). The reason for the rather low influence is that, thanks to migration (even

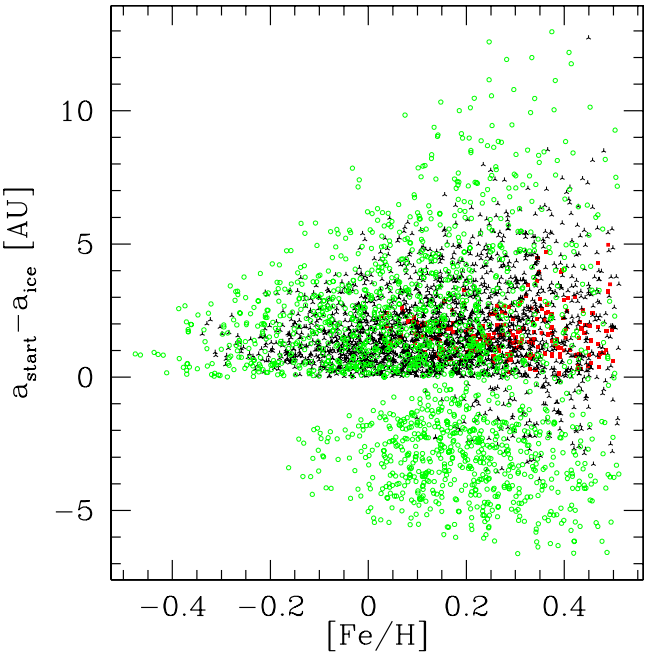

Fig. 8. Starting position relative to the ice line of embryos growing eventually to planets with a final mass $M \geq 300\,M_\oplus$ as a function of [Fe/H]. Symbols show the disk gas mass: red filled squares are low $[M_D/M_{SN}] < -0.1$. Black triangles are intermediate $[M_D/M_{SN}]$ (−0.1 to 0.4), and green open circles finally are those disk with a high mass $[M_D/M_{SN}] > 0.4$.

with the strongly reduced type I migration rate), cores never get completely cut off from a supply of fresh planetesimals to accrete. Therefore, the need for a rapidly growing gaseous envelope (where the opacity matters) in order to expand the solid feeding zone is not as important as in the case of a strict in situ formation. A growth mode that is limited only by the accretion of solids, and not the Kelvin-Helmholtz timescale of the envelope, is somewhat related to the situation for Saturn discussed in Dodson-Robinson et al. (2008). In agreement with this work we see that the reduction of the opacity is important for smaller distances $\lesssim$7 AU.

5.2. Starting position

We have seen in the last section that the location of the ice line is important for the conditions necessary for giant planet formation, and it influences in this way the birth place of giant planets. In Fig. 8 we directly plot the starting position of embryos a_{start}, which later become planets larger than 300 $M_\oplus$, relative to the position of the ice line a_{ice} in the corresponding disk, as a function of [Fe/H]. Additionally, the disk mass is color coded. In our simulation, the location of the ice line is independent of the metallicity (but dependent on Σ_0).

The figure shows that at low metallicities [Fe/H] $\lesssim -0.3$, planets can only start to form in a small region with a width of 2–3 AU just outside the ice line. In this low [Fe/H] disks, only in this region can massive cores form quickly enough. With increasing [Fe/H], the zone expands to larger radii, and for [Fe/H] $\gtrsim -0.15$, giant planets can also form inside the ice line. This corresponds, with the highest Σ_0 of the distribution (which is necessary, see next section), to a solid surface density about 3.5 times as high as $\Sigma_{S,SN}$ (also visible in Fig. 7). These results are qualitatively similar to those of Ida & Lin (2004a), except for a somewhat lower numerical value (3.5 instead of 5). The absence of red squares indicating disks with a low gas mass at negative values of $a_{start} - a_{ice}$ (i.e. inside the ice line) shows that the disk masses must always be rather high for the formation of giant planets inside the ice line, even if the metallicity is high. At [Fe/H] $\gtrsim$ 0.3, giant planets can form at almost all semimajor axes (about 1 AU to 20 AU) if concurrently $[M_D/M_{SN}]$ is high, but the preferred formation location is still beyond the ice line. Finally, at the highest [Fe/H] $\gtrsim$ 0.4, the location of the ice line becomes less important.

One therefore sees from the figure that, while at low metallicities pathways to giant planet formation are very restricted and in particular only possible in a small part of the disk, this is not the case for higher metallicities, where giant planets can form all over the disk.

5.2.1. Anti-correlation of [Fe/H] and a_{start}

There is another important chain of correlations regarding the starting positions, which cannot be seen directly in Fig. 8, but which was already mentioned in Sect. 4.3.1. For giant planet formation at low metallicities, high $[M_D/M_{SN}]$ are needed for compensation (see below). At high metallicities, in contrast, low $[M_D/M_{SN}]$ are sufficient. As the distribution of disk gas masses peaks at values that are close to the lower limit of values allowing giant planet formation, the typical $[M_D/M_{SN}]$ that leads at a high metallicity to the formation of a giant planet is a rather low $[M_D/M_{SN}]$. As seen in the figure, also at higher metallicities, the ice line remains as the typical formation location. This means that, if low disk masses correspond to low values of a_{ice} (as we assume in the nominal case), there is a negative correlation of metallicity and the typical a_{start} of giant planets-to-be. So in terms of absolute values of a_{start} (not relative to the ice line), even if giant planets also come in higher [Fe/H] environments typically from beyond the ice line, their starting positions are closer to the star in absolute terms, as the typical a_{ice} are smaller. The magnitude of this effect can be quite significant, and it corresponds to a typical difference over the 1 dex interval [Fe/H] covers of about 3 to 4 AU. If a_{ice} is, in contrast, independent of Σ_0 (which could be possible due to a dead zone that we do not include here, or if the disk is optically thin), this effect does not exist. It is therefore a finding that is sensitive to model assumptions.

5.3. Compensation effects between disk mass and [Fe/H]

Figure 9 illustrates several compensation effects in the metallicity versus gas mass plane, with disk lifetimes coded with different symbols. Each point on the graph corresponds to an initial condition which allows the formation of a giant planet ($M > 300\,M_\oplus$). Therefore, this plot shows three dimensions of the four-dimensional parameter space of initial conditions. The starting position a_{start} is projected into the plane. If we plotted all initial conditions of the population, the full area of the figure would be filled with points, distributed as a two-dimensional Gaussian distribution with means just below zero dex both for [Fe/H] (−0.02) and $[M_D/M_{SN}]$ (−0.04).

The figure shows that only initial conditions lying in the upper right-hand corner allow the formation of giant planets. The diagonal line corresponds to a solid surface density of $\Sigma_S = f_{D/G}\Sigma_0 = 6$ g/cm^2, the minimal necessary value identified in Fig. 7. That the points nearly fill the area above the line show that, in this region, any combination of the dust-to-gas ratio and the disk gas mass allows giant planet formation provided

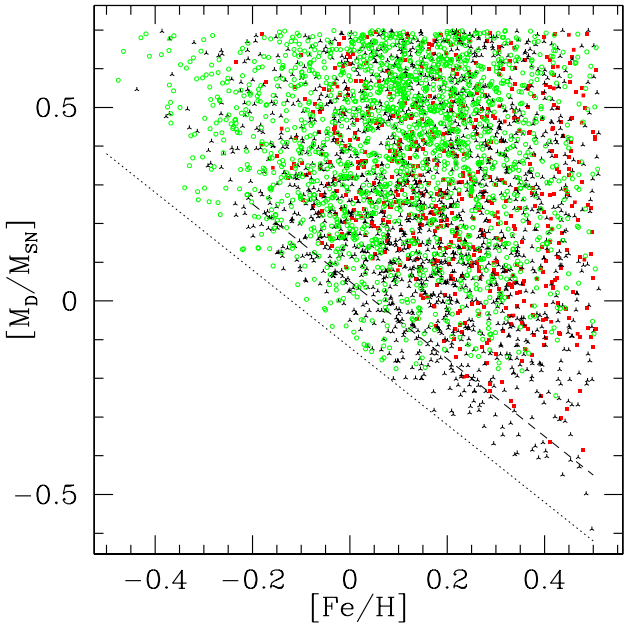

Fig. 9. Plane of initial conditions [Fe/H]-[M_D/M_{SN}] leading to the formation of synthetic planets larger than 300 $M_\oplus$. Different symbols indicate disk lifetimes: red filled squares are low $\tau_{disk} < 2$ Myr. Black triangles are intermediate τ_{disk} (2 to 4 Myr), and green open circles are disks with a long lifetime of 4 to 7 Myr. The dotted line corresponds to an initial solid surface density of 6 g/cm^2 at 5.2 AU. Between the dashed and the dotted line, no short-lived disk can lead to giant planet formation.

that the product of these two quantities gives a value above the threshold value. This means that a low disk gas mass can be compensated for by a high metallicity, and vice versa. A certain deviation of this purely multiplicative behavior can be seen at very low metallicities. There, the mechanism becomes important that the necessary very high disk gas mass is associated with such large a a_{ice} that the core formation timescale becomes very long. This is because the iceline position corresponds to the typical starting position at low metallicities. Due to this mechanism the necessary Σ_S increases stronger than in the rest of the parameter space, as discussed earlier in Sect. 4.3.

5.3.1. Comparison with observations

It is interesting to compare this result with the works of Greaves et al. (2007) and Wyatt et al. (2007). These authors have found a minimum mass of solid elements of 0.5 ± 0.1 $M_\oplus$ in a disk is needed to form giant planets. Their results are based purely on observational data (metallicities of giant planet hosts and dust disk mass distribution measured by submillimeter observations). In the model, which is in contrast built on first theoretical principles, a minimum necessary Σ_S of 6 g/cm^2 corresponds to an initial mass of planetesimals in the computational disk of about 0.4 to 0.5 $M_\oplus$. The spread comes from the position of the ice line which is not fixed by the product $f_{D/G}\Sigma_0$. This is in excellent agreement with the observed value. In the model, there is no threshold solid-disk mass of any kind built in. In our models, in contrast to Ida & Lin (2004a,b, 2005, 2008), not even a minimum core mass for the start of runaway gas accretion is built into the model. This threshold mass is not specified, but obtained by the solution of the planetary structure equations. This agreement is therefore a good indication that our core accretion model reproduces important mechanisms occurring in giant planet formation.

5.3.2. Long necessary τ_{disk} at low solid surface densities

The colors and shapes of the symbols in Fig. 9 show that there is another correlation between the initial conditions, explicitly not discussed by Greaves et al. (2007): the absence of disks with a short lifetime roughly between the dashed and the dotted line shows that near the solid surface density threshold, only long living disks can produce giant planets. This is immediately understandable within the core accretion model. Near the threshold value of Σ_S, core formation is slower than at higher solid surface densities, which can be compensated for by long disk lifetimes to still be able to form giant planets. The distribution of disk lifetimes of our synthetic disks by construction agrees with the observed distribution (Paper I). It is interesting to note further that, if the solar nebula indeed had a metallicity and [M_D/M_{SN}] close to zero dex, we can deduce from Fig. 9 that the solar nebula had a rather long disk lifetime of probably more than roughly 3−4 Myr, necessary to form Jupiter in such conditions. This in turn is in good agreement with constraints coming from a completely different measurement, namely that ages of CB chondrules and CV CAI that indicate a minimum lifetime of the solar nebula of 4.5 ± 0.8 Myr (Scott 2006).

6. Semimajor axis

In the last section, we mainly studied the effects of disk properties on planetary mass. Another important observable quantity is the final semimajor axis. As explained in Paper II, one should keep in mind that the results concerning the semimajor axis are likely to be less firm than those for the mass. The reason is first that the type I migration model we use here is still based on the isothermal Tanaka et al. (2002) migration rates, which were the only existing analytical description of type I at the time the model was written. Second we do not include any dynamical effects between multiple embryos. Nevertheless, we can gain insight into the role of several disk properties on planetary orbits in the idealized case of a single (massive) planet growing per disk in the limit of nearly absent type I migration.

6.1. Extent of migration as function of disk mass and [Fe/H]

Figure 10 shows as a function of disk gas mass (or equivalently, of the gas surface density) how far giant planets-to-be (final planetary mass higher than 300 $M_\oplus$) migrate, i.e. the difference Δa between the final semimajor axis of the planet a and the initial semimajor axis a_{start} where its seed embryo is put into the disk. Both types I and II migration rates for the planet-dominated regime, which is the most relevant one (Paper I), are proportional to the gas surface density. By construction, only inward migration is possible in the current model (Alibert et al. 2005a): For type I migration, the equations of Tanaka et al. (2002) in practice always yield negative torques, and for type II we implicitly assume to be well inside the radius of maximum viscous couple (Lin & Papaloizou 1986), which is justified in almost all circumstances (Paper I). The colors and symbols additionally show the corresponding metallicity of the disk. A quite complex pattern is seen, which is the consequence of several effects, as follows.

One expects that, at a high disk gas mass, the largest extent of migration happens. This can indeed be the case, as indicated by the dotted line. At the highest [M_D/M_{SN}], the extent of migration can be very large, up to −8 AU as seen in the lower right-hand corner of the graph. But it is more complex: when the disk mass is high, the extent of migration can also be minimal as shown by simulations in the upper right-hand corner, where

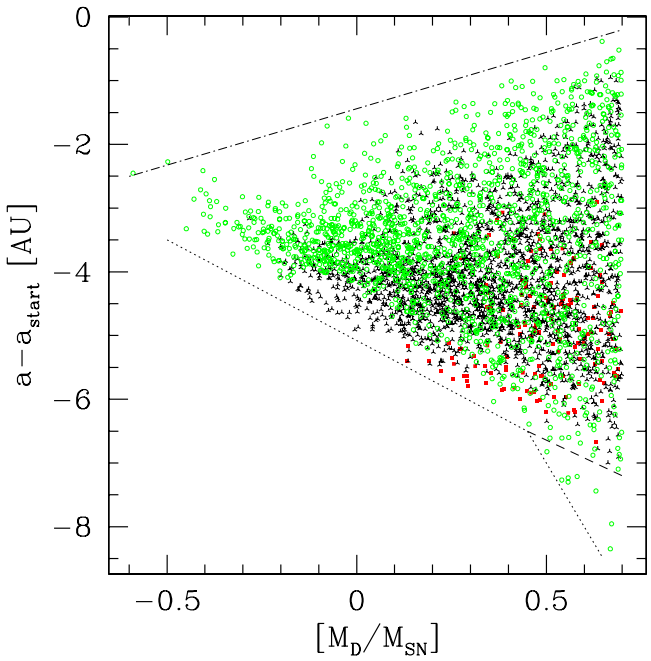

Fig. 10. Extent of migration $\Delta a = a - a_{\rm start}$ as a function of the disk gas mass $[M_{\rm D}/M_{\rm SN}]$ for synthetic planets eventually becoming giant planets ($M \geq 300\,M_\oplus$). Symbols indicate disk metallicities. Red filled squares are low [Fe/H] < -0.2 disks, black triangles are intermediate metallicity disks (-0.2 to 0.2 dex), and green open circles are disks with high [Fe/H] > 0.2. A number of lines are plotted to show relevant limiting regimes (see text).

only about 0.5 AU of radial displacement occurs. The difference comes from the metallicity, as shown by the symbols. The bottom right-hand corner contains many low [Fe/H] < -0.2 disks, which do not exist in the top right-hand corner. (Ignore for the moment the few high metallicity cases found in the outermost bottom right corner between the dashed and the dotted lines. The very large displacements ~ -8 AU there are special cases addressed further down.)

6.1.1. Braking effect

The reason for the impact of the metallicity described above is that metallicity first acts through a "braking effect". When both the gas mass and the metallicity is high, the planetesimal surface density is high. Therefore, even if the torques are strong, planets quickly get so massive (undergo quickly runaway gas accretion) that the disk soon cannot force them to migrate on the viscous timescale any more, because the planet mass is higher than the local disk mass (Lin & Papaloizou 1986). Instead, these planets quickly move into the slower planet-dominated type II migration (Armitage 2007) where the migration rate is inversely proportional to the planet mass. Therefore, if both the gas mass and the metallicity are high, and additionally the starting position of the embryo is small (which is possible in metal-rich disks as seen above), giant planets do not migrate much. We thus see that via the planet mass, a negative correlation exists between metallicity and migration, even if no influence of the metallicity on the migration rate is directly included in the model.

6.1.2. Collection effect

Second, metallicity acts through a "collection effect": when the gas mass is high, but the metallicity is low, then the extent of migration is large (cases in the bottom right corner). Under such disk conditions, the planetesimal surface density is only intermediate, but the torques are strong. Cores cannot become supercritical for gas runaway accretion in situ. To become a giant planet, they must first migrate inwards through the disk, collecting the planetesimals they come across, until they reach a mass where gas runaway accretion sets in (see the formation tracks in Paper I). Then the planet slows down due to the mentioned "braking effect". In other words, a lower planetesimal surface density and a high gas mass make planets migrate strongly, because they stay longer in the faster disk-dominated type II migration. Therefore, the extent of migration is large, from around -4 to -6 AU. The collection effect means that the minimal extent of migration (upper limit of the envelope indicated by the dashed-dotted line) increases with decreasing disk mass. The "braking" and the "collection" effect mean that accretion and migration are two interdependent mechanisms that should not be treated independently.

Third, one can again see the "compensation effect" discussed above in Sect. 5.3, i.e. that at low gas masses, high metallicities are necessary to form a giant planet. This is illustrated by the absence of low metallicity disks in the left part of the figure. At these rather low disk masses, migration is of intermediate importance, as the torques are not very strong, but at the same time the cores have to migrate over a certain distance until they have collected enough solids to get into gas runaway accretion, and slow down. Therefore, the extent of migration is intermediate at low $[M_{\rm D}/M_{\rm SN}]$, about -3 AU.

Fourth, we finally also notice a consequence of the "timescale effect" mentioned in Sect. 5.1.2. That in the outermost lower right-hand corner (between the dashed and the dotted line) all disks have a high metallicity only is the consequence of the following: to be able to migrate over such a large distance, planets must already start at large initial semimajor axes and nevertheless manage to grow supercritical on a timescale shorter than the disk lifetime. This is, however, only possible for special cases where the solid surface density is very high, or else the formation timescale for a massive core is too large. Therefore, the planets that migrate most are again found in disks with a high mass and metallicity, and with a large $a_{\rm start}$. They do not stop due to the "braking effect", as the local disk mass that is given approximately as Σa^2 is high at large distances.

6.1.3. Dependence on model assumptions

We have studied how these results depend on model assumptions, by looking at several non-nominal populations. For a population where the ice line is fixed at 2.7 AU independently of $[M_{\rm D}/M_{\rm SN}]$, the result remains quite similar.

In a non-nominal population where type II migration is only partially suppressed in the planet-dominated regime, i.e. where the reduction of the type II migration rate due to the planet's inertia is assumed to scale proportional to $(\Sigma a^2/M_{\rm planet})^{1/2}$ instead of linearly (cf. Alexander & Armitage 2009), the triangular envelope shape of the points is approximately retained, but shifted to larger extents of migration. For example, the extent of migration at the lowest $[M_{\rm D}/M_{\rm SN}]$ increases from -3 to about -5 AU, and the maximum overall distance is about -15 instead of -8 AU.

Using a type I migration efficiency factor of $f_{\rm I} = 0.1$ has a remarkably weak influence on the dependence of Δa on the disk properties, except from shifting the whole envelope of points to higher values by about -0.5 AU.

The plot also indicates that for solar-nebula like conditions ([Fe/H] and $[M_{\rm D}/M_{\rm SN}] \approx 0$), a Δa of about -4 AU is found,

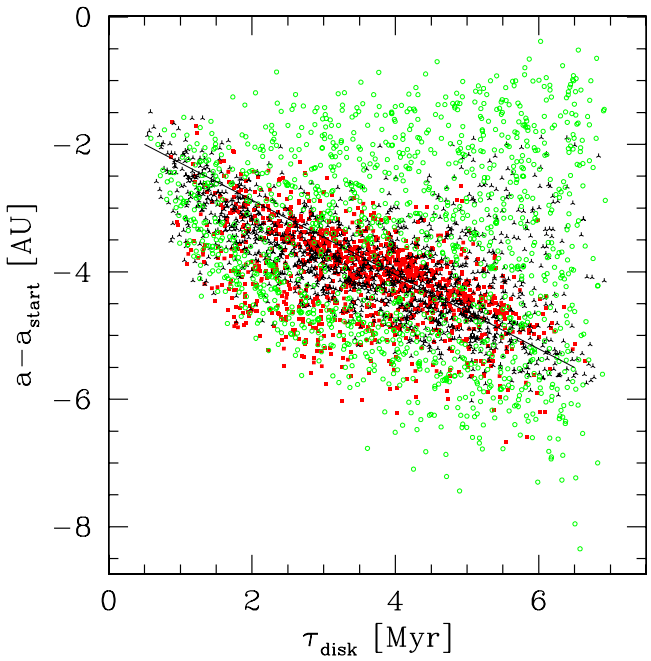

Fig. 11. Extent of migration $\Delta a = a - a_{\rm start}$ as a function of the disk lifetime $\tau_{\rm disk}$ for synthetic planets eventually ending up as giant planets ($M \geq 300\,M_\oplus$). Symbols indicate relative surface densities of planetesimals $\Sigma_{\rm S}/\Sigma_{\rm S,SN}$: red filled squares are low $\Sigma_{\rm S}/\Sigma_{\rm S,SN} < 2$. Black triangles are intermediate $\Sigma_{\rm S}/\Sigma_{\rm S,SN}$ (2 to 4), and green open circles are disks with a high $\Sigma_{\rm S}/\Sigma_{\rm S,SN} > 4$. The solid line indicates the very roughly linear behavior of Δa as a function of $\tau_{\rm disk}$. There are however large systematic departures from this simple dependence.

compatible with our earlier results for the formation of Jupiter (Alibert et al. 2005b).

6.2. Extent of migration as function of $\tau_{\rm disk}$

In Fig. 11 we have plotted the extent of migration as a function of the lifetime of the protoplanetary disk. The symbols indicate the relative amount of solids in the disk, $\Sigma_{\rm S}/\Sigma_{\rm S,SN}$, cf. Fig. 7. The boundaries for the three bins were chosen in such a way that each of the three bins contains about the same number of planets. As expected disks with a long lifetime drive migration over larger radial extents (Alexander & Armitage 2009). The plot shows that the bulk of the planets roughly lie on a line (indicated in the plot) running from $\Delta a \approx -2$ AU for the disk with the shortest lifetime that still can form a Jupiter mass planet (about 0.5–1 Myr) to a $\Delta a \approx -5.5$ AU for the disks with the longest $\tau_{\rm disk}$ of about 7 Myr. Such a relationship is expected, first because there is a characteristic locus from where giant planets come (Sect. 5.2), and second the longer the disk lifetime, the longer the torques can act to move the planet. Cases falling on the line mostly come from the intermediate bin of $2 \leq \Sigma_{\rm S}/\Sigma_{\rm S,SN} \leq 4$, which corresponds to typical values of the solid surface density.

There is however a significant spread around the diagonal line. There are, for example, at each $\tau_{\rm disk}$ simulations lying above the plotted line, i.e. where only very little migration occurs. The symbols in this area indicate that these are disks with high solid surface densities. One then finds that such cases all correspond to planets starting inside the ice line, which is possible for high $\Sigma_{\rm S}/\Sigma_{\rm S,SN} \gtrsim 3.5$, see Fig. 7. As explained in the previous section, these planets do not migrate much, because of the breaking effect that soon sets in.

On the other hand, there are also cases where clearly more migration happens than for the bulk of the planets, i.e. which lie clearly below the line. The symbols indicate that this is a mixture of both low and high solid surface densities. The former class corresponds to planets that start not far outside the ice line, but then migrate all the way down close to the star (0.1–0.7 AU), because of the "collection effect", whereas the later correspond to planets starting at very large semimajor axes, well outside the ice line, which is possible in such metal-rich disks (cf. Fig. 8), and migrate then a lot because of the braking effect setting in late at such distances, but still never end up inside ∼3 AU.

6.3. Final semimajor axis distribution of giant planets

As mentioned in the introduction, there is no clear imprint of metallicity onto the semimajor axis distribution of giant planets in the observational data, see e.g. Valenti & Fischer (2008), or Udry & Santos (2007). It has been studied repeatedly (e.g. Sozetti 2004; Santos et al. 2006) whether stars hosting a hot Jupiter are particularly metal rich, even among exoplanet hosts, manifesting in an absence of hot Jupiter host stars with a clear subsolar metallicity. A number of hot Jupiters around at least fairly low [Fe/H] ~ -0.2 to -0.4 hosts are now known, and statistical tests point to rather insignificant differences in the metallicity distribution of close-in planets and those on wider orbits (Ammler-von Eiff et al. 2009). On the other hand, planets of metal-poor stars might have a tendency to have rather large semimajor axes outside 1.5 AU (Santos et al. 2009). The basic problem is that our samples are still too small for definitive conclusions.

The lack of a clear imprint of [Fe/H] on the semimajor axis might seem surprising at first glance from a theoretical point of view considering the significant influence of [Fe/H] on $a_{\rm start}$ or Δa discussed in the previous chapters. However, as we demonstrate below, once these different effects are combined, one can actually understand such a weak dependence well on theoretical grounds.

Figure 12 shows the distribution of final semimajor axes for planets that are more massive than 300 $M_\oplus$. The planets are binned into low, medium, and high metallicity cases. Each metallicity bin was normalized individually, so the absolute heights cannot be compared between different bins. The plot shows the nominal population (left panel), and a population with $a_{\rm ice} = 2.7$ AU fixed (right panel). The "hot" planets, i.e. those planets that reach the inner border of the computational disk at about 0.1 AU, are not included here. Due to the curvature of the feeding limit, also the bins out to a distance of about 0.2 AU are artificially lowered (see Fig. 1). The planets in the feeding limit are addressed below (Sect. 7).

While the exact numerical values are different for the two populations, we see that the general shape of the semimajor axis distribution is similar, and it consists first of a slow increase in the planet frequency with increasing semimajor axis for high metallicities (or an approximately flat part for lower metallicities), then an upturn to a maximum at a few AU (at 2–3 AU on the left, at ∼1 AU on the right), followed by a gradual decline at even larger radii. This is because the core accretion timescale becomes too long at large distances (Sect. 5.1.2). Our model does not at the moment include mechanisms like scattering that could cause the planets to have larger semimajor axes. This leads to an underestimate of the number of giant planets at large distances, which is important for direct imaging searches (e.g. Bonavita et al. 2009). This issue will be addressed in forthcoming work.

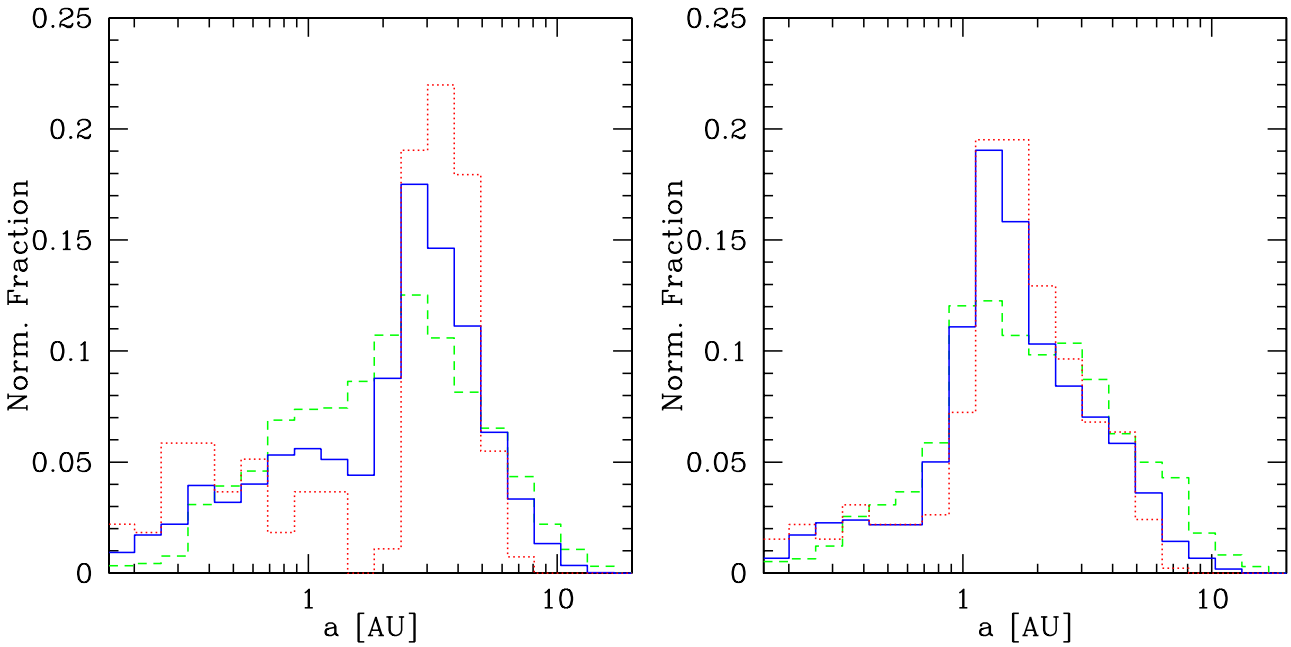

Fig. 12. Distribution of final semimajor axes of synthetic planets larger than 300 $M_\oplus$, as a function of metallicity. In both panels, the red dotted lines are for [Fe/H] < −0.2, the blue solid lines for −0.2 < [Fe/H] < 0.2, and green dashed lines for [Fe/H] > 0.2. The *left panel* is the nominal population, while the *right panel* is a population where $a_{\rm ice}$ = 2.7 AU fixed for all initial conditions. Hot planets ($a \lesssim 0.1$ AU) are not shown in this figure.

6.3.1. Imprint of the iceline

For the nominal population, the location of the peak can be roughly understood by considering some relevant mean values (median values give similar results) for the planets with a final mass >300 $M_\oplus$: first, the mean Σ_0 of these planets is about 480 g/cm^2, corresponding to an $a_{\rm ice} \approx 5.5$ AU. As indicated by Fig. 8, the mean starting position should be somewhat outside of this distance. The measured mean $a_{\rm start}$ is indeed 6.5 AU. The mean disk lifetime of 3.8 Myr corresponds to a mean $\Delta a \approx -3.8$ AU (Fig. 11), so that we estimate a mean final semimajor axis of 2.7 AU, which is the same as the mean value found in the simulations. This corresponds approximately to the peak of the distribution of the intermediate metallicity bin, which is the bin with the highest number of planets in it. Thus, the peak of the distribution is due to the fact that there is a typical locus from where planets come, combined with a typical distance over which they migrate.

This imprint of the ice line into the semimajor axis distribution is confirmed by the right-hand panel, where $a_{\rm ice}$ is at 2.7 AU for all disks. Compared to the nominal case, the upturn in the distribution is found at a smaller semimajor axis, namely at about 1 AU which might be closer to the observed distribution and might also be sharper, at least for the high-metallicity bin. These differences can be understood. The sharpness is a logical consequence because part of the spread in the typical $a_{\rm start} \gtrsim a_{\rm ice}$ is now simply eliminated by suppressing the dependence of $a_{\rm ice}$ on Σ_0. That the upturn happens at a smaller distance simply comes from the fact that an $a_{\rm ice}$ = 2.7 AU is clearly less than the mean $a_{\rm ice}$ in the nominal case (5.5 AU). We conclude that there is a correlation between the position and shape of the upturn in the planetary semimajor axis distribution and the thermodynamic properties in the protoplanetary disk, which is an interesting result.

6.3.2. Comparison with observations and predicted decrease

Here we only consider the condensation of ices as a mechanism causing a preferred location for giant planet formation. Other (or additional) mechanisms with comparable consequences could also be at work in the disk (cf. Schlaufman et al. 2009). One should also keep in mind that the temperature and solid surface density structure of protoplanetary disks is likely much more complex than assumed in the simple α models used here (Dzyurkevich et al. 2010). This means that the result that the frequency of giant planets is an increasing function of the semimajor axis inside a few AU is a more robust prediction than the specific shape and cause of it. Observationally, after correcting the observational bias, an overall distribution of the semimajor axes of giant planets similar to the one here has been found recently (Mayor et al. 2011). No imprint of the metallicity is seen in the still small dataset, where no fine structures (like e.g. the small valley visible at low metallicities just inside the upturn) could currently be seen. It should be noted that such fine structures are sensitive to specific model assumptions.

The baseline of the RV surveys is also not long enough yet to determine whether the theoretically predicted decrease at larger distances (≳5 AU) exists. Such a decrease can, in contrast, be seen as a solid prediction of the core accretion theory. The observational test of this will be an important constraint for the core accretion model, since it is linked to the core-growth timescale. A complication arises from the ability of the gravitational interaction of several giant planets to lead to the scattering of bodies to larger semimajor axes. This evolutionary effect will blur the timescale limit set during formation. To still be able to use the observational constraint, formation and evolution through N-body interaction must be coupled self-consistently (Alibert et al., in prep.).

6.3.3. Independence from [Fe/H]

Comparing the three metallicity bins in the nominal case, we see that there are some visible, but not extreme differences. For the low-metallicity bin, one sees that this distribution is rather flat inside about 3 AU, then has a sudden upturn, followed again by a sharp downturn. Thus, the planets are mostly well confined

Table 1. Mean starting position $a_{\rm start}$, extent of migration Δa, and final semimajor axis a for planets with a final mass higher than 300 $M_\oplus$, as a function of metallicity.

Metallicity	$a_{\rm start}$ [AU]	Δa [AU]	a [AU]
[Fe/H] > 0.2	6.2	–3.5	2.7
−0.2 < [Fe/H] < 0.2	6.7	–4.0	2.7
[Fe/H] < −0.2	7.5	–4.9	2.6

Notes. Planets inside 0.1 AU are excluded.

Table 2. Mean [Fe/H] of the initial conditions leading to different types of synthetic planets.

Mean [Fe/H]	Nominal	$f_{\rm I} = 0.1$
All planets (initial cond.)	–0.02	–0.02
Hot, $M/M_\oplus < 6$	0.00	0.00
Hot, $6 < M/M_\oplus < 100$	0.05	0.06
Hot, $M/M_\oplus > 100$	0.08	0.17

to a particular region. For the high-metallicity bin, and to a lesser extent also for the intermediate metallicities, the increase at small semimajor axes is more gradual towards the peak, and also the decrease towards the even larger semimajor axis is less abrupt, which means that the high-metallicity distribution has more planets both at smaller and larger distances than the low-metallicity one.

These finding come from giant planets around metal-poor stars only forming within a well-defined region, namely at the sweet spot for giant planet formation as was shown in Sect. 5.2, in contrast to higher metallicities. Considering the location of the peak for the low-metallicity bin, one notes that the peak of giant planets around low-metallicity stars is found somewhat farther out (about 1 to 3 AU) than for the higher metallicity cases. This might be in accordance with the observational findings of Santos et al. (2009). This can also be understood in terms of our findings from the previous sections. At low metallicities, giant planets must come from outside the ice line (Sect. 5.2), i.e. from a significant distance. At the largest semimajor axes ($a \gtrsim 6$ AU), however, the relative frequency of more metal-rich planets is again higher. This is a consequence of the timescale effect: a lot of solids are necessary to form a core in time at large distances, and this is not the case at low metallicities.

These reasonings alone are, however, not yet able to explain the observed (and theoretical) semimajor axis distribution with its weak [Fe/H] dependence, as it would rather imply a strong absence of giant planets around low-metallicity stars at small semimajor axes. The missing link is the anti-correlation of metallicity and the extent of migration (Sect. 6.1), due to the "braking effect", which stops migration quicker in a metal-rich disk, and the "collection effect", which enhances it in solid poor ones. Thus, while giant planets initially arise closer-in in high [Fe/H] environments, they migrate less, while for low [Fe/H], they start farther out, but migrate more.

These findings can be quantified (Table 1). For the nominal population, the mean $a_{\rm start}$ is 6.2, 6.7 and 7.5 AU for the high, medium, and low [Fe/H] group. But the mean Δa is −3.5, −4.0 and −4.9 AU again for high, medium, and low [Fe/H], which results in a near cancellation of the two counteracting effects, so that the resulting mean final semimajor axis for the three metallicity bins are all the same except for a tiny difference of 0.1 AU. Observationally, these three mean values appear indistinguishable. Thus, a complex of interplay of migration and accretion explains the observed absence of a strong correlation of metallicity and semimajor axis for extrasolar giant planets.

7. Metallicity of close-in Jovian and Neptunian planets

7.1. Observed distribution

Early detections made with high-precision radial velocity observations (Udry et al. 2006) suggest that the distribution of the host star metallicities of close-in lower mass Neptunian and super-Earth planets follows a different pattern than observed for hot Jupiters, namely that their metallicity distribution is not shifted towards the higher metallicities. This result has been subsequently discussed in several studies (e.g. Sousa et al. 2008; Ghezzi et al. 2010a) and recently confirmed (Mayor et al. 2011; Sousa et al. 2011).

The latter authors find that the mean metallicity of FGK hosts stars is positively correlated with the mass of their most massive planet. They find a mean [Fe/H] of −0.11, 0.04, and 0.10 dex for host stars having planets with masses between 0.01 and 0.1 $M_{\rm J}$, 0.1, and 1 $M_{\rm J}$ and >1 $M_{\rm J}$, respectively. In a similar way Ghezzi et al. (2010a) show that for FGK host stars, in the observational data, there is an offset in the mean metallicity of +0.11 dex by which Jovian planet hosts are more metal-rich than stars that only host Neptunian planets. The probability that the two samples are drawn from the same parent distribution is, however, found to be 17%, i.e. clearly non-negligible. They give a mean metallicity for Neptunian planet only FGK hosts of 0.01 dex, and of 0.12 dex for Jovian planet FGK hosts.

7.2. Synthetic result

It is obvious that these observations raises the question whether such a relation exists for the synthetic population, too. From Sect. 4.1 such a behavior is expected, but the problem is that there, the mass function is shown for all semimajor axes, while the observed planets with $M \leq 30\,M_\oplus$ are almost all inside of a few 0.1 AU.

We therefore plot in Fig. 13 the metallicity distribution[2] of those synthetic planets that have migrated into the feeding limit at about 0.1 AU ("Hot" planets), for three different mass bins: $M > 100\,M_\oplus$, $100 > M/M_\oplus > 6$, and $M/M_\oplus < 6$. The lower limit of 6 $M_\oplus$ approximately reflects the lower limit to which the model should yield masses that are not too much affected by the initial conditions (Paper I). Below this limit we can still conclude that there are additional low-mass planets, but their final mass is not described well in the model. The upper two panels in Fig. 13 show the nominal population with a type I efficiency factor $f_{\rm I} = 0.001$, while the two lower panels show a non-nominal population with $f_{\rm I} = 0.1$. Numerical values for the mean metallicity of the different subpopulations are listed in Table 2.

In all figures, the black line additionally shows the [Fe/H] distribution of all synthetic planets for comparison, and thus the distribution from which the initial conditions are drawn. It is a Gaussian with a mean $\mu = -0.02$ dex and a dispersion $\sigma = 0.22$ dex (cf. Paper I).

One notes that for both populations, the hot Jovian planets have a distribution that is more metal rich than the intermediate-mass and Neptunian planets or the super-Earth planets. For the

[2] By "metallicity" of a planet we always refer in this work to the disk/stellar [Fe/H] of the initial conditions that lead to the formation of this planet, and not to the heavy element abundance in the planet itself.

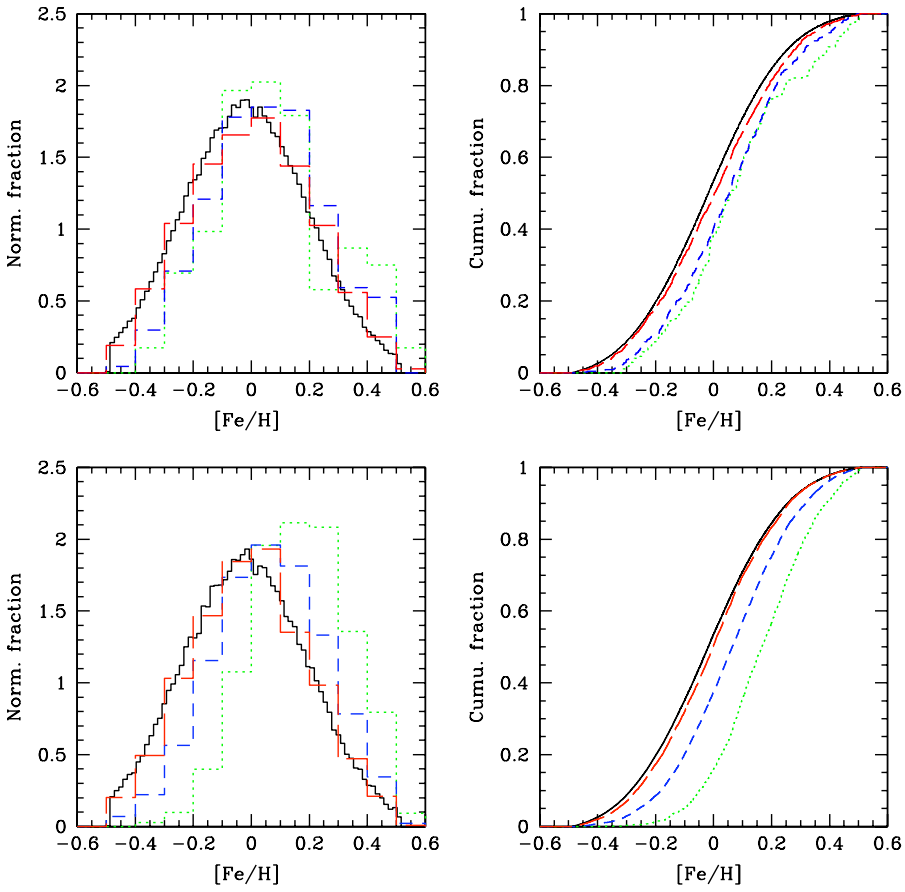

Fig. 13. Histogram and cumulative distribution of the metallicity of close-in synthetic planets. The two upper panels are for the nominal population ($f_I = 0.001$), the lower two for a population with a faster type I migration ($f_I = 0.1$). In all panels, green lines stand for massive planets ($M > 100\,M_\oplus$), the blue lines for planets with $100 > M/M_\oplus > 6\,M_\oplus$, and red lines are for low-mass planets ($M/M_\oplus < 6$), all inside the feeding limit, i.e. inside about 0.1 AU. The black lines serves for comparison and shows the metallicity distribution of all synthetic planets (at all semimajor axes) and thus simply the distribution from which we draw the initial conditions.

nominal distribution, the difference between the intermediate and the high-mass bins is, however, extremely small, except for a possible excess of hot Jupiters with high metallicity $\gtrsim$0.2 dex. In terms of mean metallicities, the difference is just 0.03 dex. For the population with $f_I = 0.1$, the situation is quantitatively quite different: Here, the mean metallicity of the Jovian mass bin is with 0.17 dex clearly higher (+0.11 dex) than the middle bin with the Neptunian planets (0.06 dex). For the lowest mass bin, which contains the prototerrestrial planets, a vanishingly small offset to the distribution from which the initial conditions are drawn is seen for both synthetic populations, because these planets have a mean of [Fe/H] = 0.00.

We thus see, as expected, that the mean metallicity increases with increasing planetary mass. Quantitative results, however. depend on poorly constrained model parameters like f_I. The large difference for the mean metallicity of Jovian planets for the two populations stems in particular from the following. Giant planets forming in high metallicity and low gas mass environments inside the ice line do not usually migrate into the feeding limit provided that type I migration is negligible ($f_I = 0.001$), because of the very efficient braking effect in type II migration at such small semimajor axes (Sect. 6.1). They instead stay at distances between roughly 0.4 and 1 AU. For $f_I = 0.1$ this is different. There, type I migration, which has a migration rate that in contrast increases linearly with planet mass, brings the quickly growing cores starting inside the ice line so close to 0.1 AU, that many planets eventually end up as hot Jupiters. This causes the high mean metallicity.

For a third population with $f_I = 0.001$, but only partially suppressed type II migration, one finds results for the metallicities that approximately lie between the two cases discussed here. This means that the metallicity distribution of hot Jupiters is a measure of the efficiency of both types I and II migration. In summary we see that the synthetic populations reproduces the general observed trend, but that the more specific results depend on uncertain model settings like the efficiency of migration.

8. Planet frequency

Comparing observed and theoretical detection probabilities $P_{\rm det}$ of planets as a function of some input (disk) variable is a classical application of population synthesis calculations (e.g. Ida & Lin 2004b; Kornet et al. 2005; Dodson-Robinson et al. 2006; Matsuo et al. 2007). Here we study the frequency of giant planets as a function of [Fe/H], $M_{\rm disk}$, and $\tau_{\rm disk}$.

8.1. [Fe/H]: influence of the gas mass

In Paper II, we compared the synthetic "metallicity effect" (the increase of the detection rate of giant planets with host star [Fe/H]) to the observed one and found that the synthesis can reproduce this important observational constraint. Here we focus on another aspect, namely how the "metallicity effect" depends on the amount of gas present in a protoplanetary disk.

For simplicity, we again assume here that a planet can be detected by the radial velocity method if it induces a velocity semi-amplitude K larger than 10 m/s, and if its orbital period is less than 10 years. We thus focus on giant planets. The left-hand panel of Fig. 14 shows the detection probability as a function of metallicity if additionally the gas mass Σ_0 of the corresponding disk is either higher than some lower limit, or lower than some upper limit. In all cases, the detection probability $P_{\rm det}$([Fe/H],Σ_0)

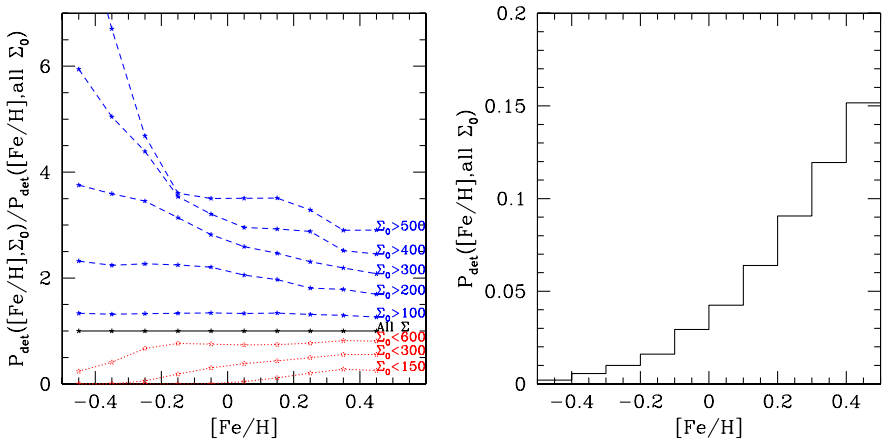

Fig. 14. *Left panel*: detection probability as a function of metallicity and gas surface density. The plot shows the relative detection probability as a function of [Fe/H] for disks that have Σ_0 meeting the condition indicated in the plot, normalized by the P_{det}([Fe/H], all Σ_0) i.e. the detection probability as a function of [Fe/H] alone, including all Σ_0. This quantity is plotted in the *right panel*. A curve in the left panel that increases towards the low [Fe/H] (blue lines) therefore means a less strong metallicity effect, while a curve that decreases towards the low [Fe/H] (red lines) indicates a stronger metallicity effect. The instrumental accuracy is 10 m/s.

obtained in this way was divided by the detection probability at a given metallicity but including all Σ_0, i.e. the (usual) detection probability as a function of metallicity alone. This quantity is shown in the right-hand panel of Fig. 14. Like that, the differential influence of the gas mass on P_{det} is shown.

One notes that for disks that have Σ_0 above a certain threshold, i.e. where the most gas poor disks are excluded, the normalized probability is greater than 1, which means that more planets are detected. When only a moderate lower limit is used ($\Sigma_0 > 100$ g/cm^2), the increase is only small and nearly identical for all metallicities. However, the higher the Σ_0 threshold becomes, the more a dependence on [Fe/H] develops. The relative increase of P_{det} is highest for the subsolar metallicities. In other words, the metallicity effect is weakened, if the protoplanetary disks are gas rich. A mirrored effect is seen if only disks with a mass lower than some Σ_0 are considered, so that the most gas-rich disks are now excluded. Here, the relative decrease in P_{det} is strongest for the low [Fe/H] bins, which means that the metallicity is strengthened if the protoplanetary disks are gas poor.

These findings are clearly a consequence of the "compensation" effect discussed theoretically in Sect. 5.3. In a gas-rich environments, lower metallicities are sufficient to allow giant planet formation.

8.2. Disk gas mass

Figure 15 shows the percentage of stars (initial conditions) where the formation of a giant planet with a mass of at least 100 $M_\oplus$ is possible, as a function of the initial disk gas mass measured as [M_D/M_{SN}]. The lowest value of about −0.6 (Σ_0 = 50 g/cm^2) corresponds to an initial content of gas within the computational disk of about 0.004 $M_\odot$. The upper limit of about 0.7 (Σ_0 = 1000 g/cm^2) corresponds to a disk with an initial mass of 0.09 $M_\odot$. As the individual primordial disk mass is unknown for the Gyr old stars around which extrasolar planets are typically discovered, we directly plot the real frequency, without taking any observational bias into account, in contrast to the results for [Fe/H].

As expected from Sect. 4.1, one sees that the frequency of giant planet increases with [M_D/M_{SN}]. For [M_D/M_{SN}] $\gtrsim$ −0.1, the increase is found to be slightly stronger than linear with the disk mass. An approximate fit to the data is given as $0.04 \times (M_{disk}/0.017\ M_\odot)^{1.2}$. For lower disk masses, this fit overestimates the number of giant planets. We note that two quantities that are important for giant planet formation scale with similar exponents: the core accretion rate scales linearly with the

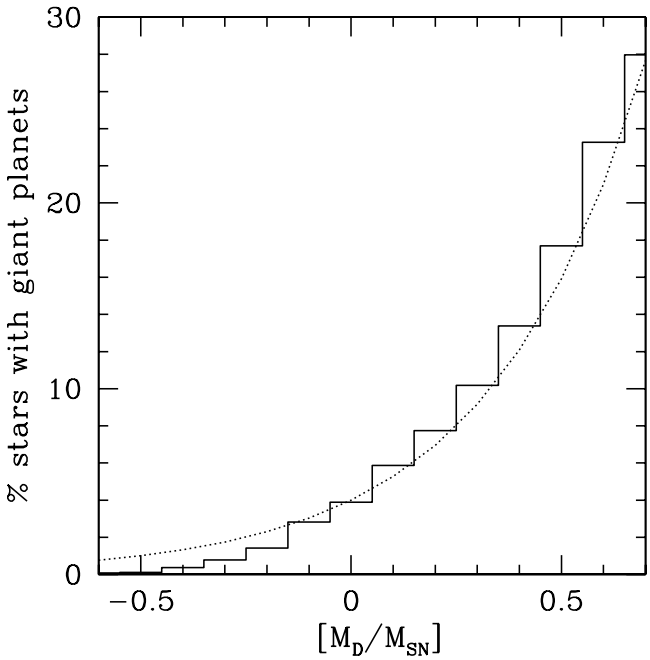

Fig. 15. Percentage of stars having a giant planet with a mass of at least 100 $M_\oplus$ as a function of the initial disk gas mass. The dotted line scales as $M_{disk}^{1.2}$.

planetesimal surface density Σ_S which is itself proportional to the disk gas mass ($\Sigma_S = f_{D/G}\Sigma_0$), while the isolation mass is proportional to $\Sigma_S^{1.5}$ (e.g. Lissauer et al. 1993).

For the most massive disks considered in this work, one finds a frequency of about 28%. This is in fair agreement with the result of ∼35% of Dodson-Robinson et al. (2006) at the same disk mass. At lower disk masses we find somewhat higher frequencies than these authors. The reason for this difference could be that migration was not included in Dodson-Robinson et al. (2006) so that higher surface densities are necessary (cf. Sect. 5.1).

8.3. Disk lifetime

Figure 16 shows the percentage of stars with a giant planet ($M \geq 100\ M_\oplus$) as a function of disk lifetime τ_{disk} for the nominal population. Not surprisingly, there is a positive correlation of the disk lifetime and giant planet occurrence, as in a longer living disk, cores have more time to grow to a size where they

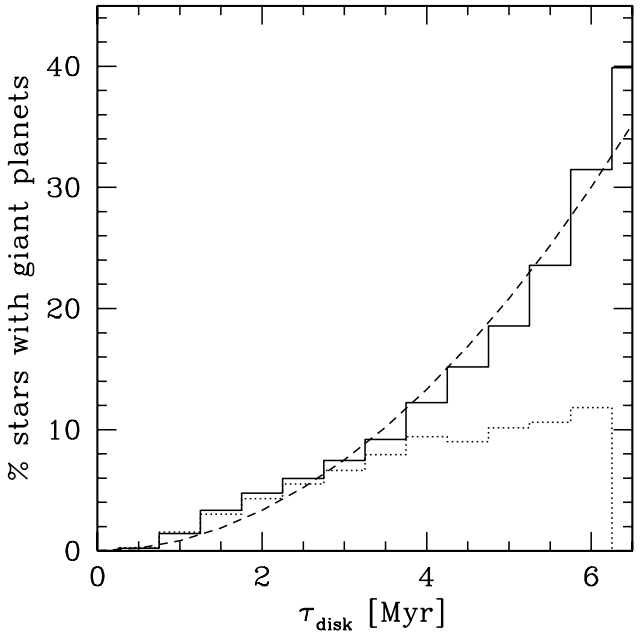

Fig. 16. Percentage of stars having a giant planet with a mass of at least 100 $M_\oplus$ as a function of the disk lifetime $\tau_{\rm disk}$. The solid line shows the nominal population, while the dotted line corresponds to a population where disk mass and disk lifetime are not correlated (cf. Sect. 9). The dashed lines scales as $\tau^2_{\rm disk}$.

can trigger gas runaway accretion. An approximate fit to the frequency is given as $0.075\times(\tau_{\rm disk}/3\,{\rm Myr})^2$. The strong dependence on $\tau_{\rm disk}$ is caused by the double role of $\tau_{\rm disk}$ both as a threshold and as a factor directly influencing the planet mass, as described in Sect. 4.1.

For the disk with the longest $\tau_{\rm disk} \approx 6.5$ Myr, the percentage of stars with a giant planet is remarkably high at about 40%. For comparison, Dodson-Robinson et al. (2006) find about 30% for such a $\tau_{\rm disk}$. This high fraction, however, depends on a disk mass-disk lifetime correlation inherent in the initial conditions, as addressed in Sect. 9 below.

Recently, it has been discussed whether extrasolar-planet host stars show a stronger depletion in lithium compared to non-planet hosts. No general agreement exists currently on this question on observational bases, with analyses both in favor of (Israelian et al. 2009; Sousa et al. 2010) or against (Baumann et al. 2010; Ghezzi et al. 2010b) such a correlation. On theoretical bases, several mechanism can enhance lithium depletion (e.g. Baraffe & Chabrier 2010). A possible explanation based on the star rotational history, which is interesting in the context here, has been put forward by Bouvier (2008). In this model it is assumed that long disk lifetimes lead via disk locking to a slower initial rotation of the star at the ZAMS. This causes a phase of stronger differential rotation between the radiative core and the convective envelope, which is in turn responsible for enhanced lithium depletion.

If the correlation of enhanced lithium depletion and the presence of massive planets can indeed be confirmed, then the lines of reasoning of Bouvier (2008) provides a way of relating disk lifetime and the formation probability of giant planets. The result shown here that giant planets preferentially form around disks with long lifetimes fits in this picture well. In the direct gravitational collapse model for giant planet formation, this is not the case.

The abundance of lithium would then provide a link that is observable today between primordial disk properties ($\tau_{\rm disk}$) and planet occurrence in a similar, although much more indirect, way than the metallicity. We comment that long disk lifetimes are in particular needed for giant planet formation when the metallicity is on the low side ([Fe/H] $\lesssim -0.2$), while at high [Fe/H], short lifetimes ($\tau_{\rm disk} \lesssim 2$ Myr) can be sufficient, as demonstrated in Sect. 5.3.2, so that the planet frequency-$\tau_{\rm disk}$ correlation also depends on [Fe/H].

9. Disk mass – disk lifetime correlation

When generating initial conditions, we first draw in the nominal procedure the gas surface density Σ_0 and then, independently of it, the photoevaporation rate $\dot{M}_{\rm w}$. This procedure has the side effect that disks with a high initial gas surface density Σ_0 will on average also have a longer lifetime $\tau_{\rm disk}$, because for the same $\dot{M}_{\rm w}$ more massive disks live longer. Thus, there is a positive correlation between disk mass and lifetime.

To assess the consequences of this correlation, we generated an alternative set of non-nominal initial conditions in the following way. After drawing Σ_0, we directly draw a $\tau_{\rm disk}$ from a specified distribution and then choose the $\dot{M}_{\rm w}$ that is necessary to get this $\tau_{\rm disk}$, for the given Σ_0 (and the fixed α). Like that, no correlations exist any more between Σ_0 and $\tau_{\rm disk}$. Instead, Σ_0 and $\dot{M}_{\rm w}$ are now positively correlated, which could arise in a situation where photoevaporation by the central star is dominant, even though, strictly speaking, the functional form of the photoevaporation would then be different than assumed in our disk model (Matsuhama et al. 2003).

The distributions we have used for $\tau_{\rm disk}$ for the non-nominal case are either (i) a uniform distribution of lifetimes between 0 and 6 Myr, which corresponds to the linearly decreasing fraction of stars that have a JHKL excess as a function of mean cluster age in Haisch et al. (2001), or (ii) an exponential decrease of this fraction with time as $\exp(-t/2.5\,{\rm Myr})$, which is based on more recent compilations of disk lifetimes, such as in Mamajek (2009) or Fedele et al. (2010).

9.1. Effect on giant planet frequency

We have found that the impact of using this different prescription only has minor impact on the general properties of the synthetic population as compared to the nominal case. This regards, in particular, the distribution in the mass-distance plane, the migration behavior, or the general shape of the PIMF. The difference between the linear and the exponential distributions for $\tau_{\rm disk}$ is even smaller.

Only when we directly plot the frequency of planets as a function of disk lifetime as in Fig. 16 does a significant difference become visible. In this figure, the percentage of stars with a giant planet for the non-nominal case with the linear distribution is shown. One notes that, while for the nominal case, a clear increase in the giant planet frequency with disk lifetime is seen for $\tau_{\rm disk} \gtrsim 4$ Myr, this is not the case for the population without a correlation between $\tau_{\rm disk}$ and $M_{\rm disk}$. The reason for this is that in the non-nominal case, there are many disks with long lifetimes, but still only such small gas masses that giant planets cannot form, which reduces the fraction. In the nominal population, disks with high $\tau_{\rm disk}$ usually also have high Σ_0, which both contribute to successful giant planet formation.

10. Summary and conclusion

We have extensively studied the influence of some of the most important properties of protoplanetary disks of solar-like stars

(disk metallicity [Fe/H], disk (gas) mass $M_{\rm disk}$, and lifetime $\tau_{\rm disk}$) on the planets growing in them. We have found numerous correlations, which we summarize here.

We first give a list of the most central correlations between disk and planetary properties as found within the core accretion paradigm, which are less sensitively to model settings. From an observational point of view, we have to distinguish two classes: first, correlations that can be tested against observations, as they involve the (stellar) [Fe/H]; second, correlations that are linked to the disk mass and lifetime. These primordial disk properties cannot be directly observed, even though some pathways that at least approximately determine them might arise in future. The correlations involving the metallicity are

1. The planetary initial mass function for metal-rich disks contains a higher number of giant planets, but their mass is not significantly higher. Metallicity mostly acts as a threshold for giant planet formation, but is not correlated with the mass of giant planets, except for rare special cases (point 4).
2. No clear metallicity effect (positive correlation of the detection rate of planets with stellar [Fe/H]) is found in the Neptunian mass domain. At even lower masses, an anti-correlation could exist.
3. Observationally, at a low radial velocity precision i.e. for giant planets, no clear correlation of [Fe/H] and the planetary mass distribution is visible. At high precision (∼1 m/s), in contrast, a systematic anti-correlation of [Fe/H] and the Neptunian-to-Jovian planet ratio becomes detectable: The lower [Fe/H], the higher the ratio of Neptunian to Jovian planets.
4. The most massive companions ($\gtrsim$10–20 $M_\oplus$) cannot form by core accretion at clearly subsolar metallicities, since core-growth then takes so long that disks are significantly depleted once the cores trigger gas runaway accretion. In the supersolar regime, maximum planet masses are, in contrast, independent of [Fe/H]. Such planets are, however, very rare.
5. The absence of a strong correlation of metallicity and the semimajor axis distribution of giant planet is explained as follows. Around metal-poor stars, giant planet cores can only form in a gas-rich disk and at large distances $a_{\rm start} \gtrsim a_{\rm ice}$. These high disk gas masses drive migration over larger distances, tending to cancel out the large $a_{\rm start}$. In a metal-rich disk, it is the opposite: giant planets can also form at shorter orbital distances. But since low gas masses are sufficient, planets also migrate less. These correlations of accretion and migration explain the observed weak dependence. In short, at low [Fe/H], planets start further out, but migrate more, while at high [Fe/H] they start closer in, but migrate less.

The correlations involving the disk mass and lifetime are

1. The planetary initial mass function for massive gas disks contains more giants planets with a higher mass, but less giants with a lower mass. Disk gas masses and giant planet masses are correlated.
2. Disk lifetimes both act as a threshold (like [Fe/H]) for giant planet formation and influence the final total mass (like $M_{\rm disk}$), so that they have a strong influence on the giant planet population.
3. Maximal planetary masses and disk mass are in contrast to the situation for [Fe/H] correlated over the full range of disk masses. Except for very low disk masses, maximum possible planet mass and disk mass correlate linearly. There is a wide spread in the efficiency of converting disk gas in envelope mass, but to an order of magnitude, it is 10%.
4. Low metallicities (i.e. dust-to-gas ratios) can be compensated for by high disk masses to allow giant planet formation, and vice versa ("compensation effect"). The lowest necessary total solid content in a disk for giant planet formation is about 0.4 to 0.5 $M_\oplus$.
5. The metallicity effect is weaker when disk gas masses are high, and stronger if they are small. This is a consequence of the metallicity-disk gas mass "compensation effect".
6. Near the solid surface density threshold necessary for giant planet formation, long disk lifetimes of at least 3–4 Myr are necessary. This could indicate that the solar nebula probably had a rather long lifetime.

We also found the following correlations, which are either of second order, or could be dependent in a more significant way on specific model assumptions:

1. There is an imprint of the disk mass distribution on the upper end of the planetary mass function.
2. The chain of correlations of low [Fe/H] $\Rightarrow$ high necessary gas mass $\Rightarrow$ large $a_{\rm ice}$ $\Rightarrow$ large typical $a_{\rm start}$ means that in low [Fe/H] disks, embryos of giant planets come typically from farther out. The opposite applies for high [Fe/H].
3. For giant planet formation, low metallicities cannot be compensated by high gas masses ad infinitum, at least if higher mass disks have an ice line farther out due to stronger viscous dissipation. The sweet spot for giant planet formation at $a_{\rm start} \sim a_{\rm ice}$ moves then so far out that the increasing core-growth timescale can no longer be compensated for by increasing the disk mass.
4. The semimajor axis distribution of giant planets outside 0.1 AU first consists of a nearly flat part, followed by an upturn. The location of the upturn probably depends on the location of the ice line. It is because there is a typical locus from where giant planets come, combined with a typical distance over which they migrate. Disk thermodynamical properties thus leave an imprint on the planetary semimajor axis distribution.
5. The extent of migration of giant planets $\triangle a = a - a_{\rm start}$ is large (∼−6 AU) in gas-rich disks with a low [Fe/H]: Torques are strong, $a_{\rm start}$ are large, and cores must migrate over a large distance until they have collected sufficient planetesimals to trigger gas runaway accretion and slow down in slow planet-dominated type II migration. The extent is minimal ($\lesssim$−1 AU) in gas and solid rich disk and if the embryo starts inside $a_{\rm ice}$: giant planets grow rapidly and local disk masses are low, so that planets soon stop due to their inertia. For low-mass disks $\triangle a \sim -3$ AU, and for disks similar to the MMSN, $\triangle a \sim -4$ AU.
6. The extent of migration of giant planets increases with disk lifetime $\tau_{\rm disk}$. Very roughly, there is a linear correlation. For disks with the shortest $\tau_{\rm disk} \approx 0.5$ Myr still allowing giant planet formation, $\triangle a$ is ∼−2 AU, while in the longest living disks ($\tau_{\rm disk} \approx 7$ Myr), $\triangle a \sim -5.5$ AU. There are important systematic departures from this correlation depending on the solid content of the disk.
7. Observationally, hot Jupiters are found around higher metallicity hosts than lower mass close-in Neptunian and super-Earth planets. This is also found in the synthetic population. The degree of difference correlates positively with the efficiency of type I migration and varies between 0.03 and 0.11 dex for the mean [Fe/H] values.

Finally, with the following points we mostly confirm earlier results concerning the relationship of disk properties and planet

properties. The quantitative results often differ to a certain degree, but qualitatively they are the same (cf. Ida & Lin 2004a,b; Dodson-Robinson et al. 2006; Kornet et al. 2006; Matsuo et al. 2007; Thommes et al. 2008).

1. Comparison with observation shows that the very large majority of known extrasolar planets lie in the [Fe/H]-mass domain populated by the core accretion formation mechanism.
2. The preferred location for planet formation is at about 5 AU. The minimal necessary surface density of planetesimals to allow giant planet formation is about $\Sigma_S = 6$ g/cm^2 there. Both in- and outside this distance, higher Σ_S are necessary: inside to overcome the low isolation mass, outside to overcome the long core-growth timescale.
3. At metallicities [Fe/H] $\lesssim -0.1$, giant planets can only form in an annulus of 2–3 AU in width outside the ice line $a_{\rm ice}$. With increasing [Fe/H], giant planets can also form in- and clearly outside $a_{\rm ice}$, but the ice line remains the preferred starting position. Only at the highest [Fe/H] $\gtrsim 0.4$, does the location of $a_{\rm ice}$ become less important, and giant planets can form all over the disk from ∼1 to ∼20 AU.
4. The fraction of stars with a giant planet as a function of initial disk mass is found to be approximately $0.04 \times (M_{\rm disk}/0.017\ M_\odot)^{1.2}$.
5. The fraction of stars with a giant planet as a function of disk lifetime is found to be roughly $0.075 \times (\tau_{\rm disk}/3\ {\rm Myr})^2$. A possible link between giant planet occurrence and lithium depletion in the host star could be an observational manifestation of this correlation. The influence of $\tau_{\rm disk}$ on the frequency of giant planets is, however, much reduced if the disk mass and lifetime are not positively correlated, as implicitly assumed in the nominal population.

This long list of correlations clearly indicates the strong dependence of planet formation on protoplanetary disk properties. It calls for profound improvements of the disk models used in planet formation simulations, for a rigid inclusion of observational results on disks in the initial conditions, and for the incorporation of observations of disks like SEDs as additional constraints for planet formation models.

Such improvements of the initial and boundary conditions for planet formation will in the end allow a better understanding of the planet formation process itself.

Note: The numerical data of the nominal synthetic population can be obtained in electronic form at `http://www.mpia.de/homes/mordasini/Site7.html`

Acknowledgements. We thank Stephane Udry, Chris Ormel, and Kai-Martin Dittkrist for useful discussions. C. Mordasini acknowledges the financial support as a fellow of the Alexander von Humboldt foundation. This work was supported in part by the Swiss National Science Foundation. Yann Alibert is thankful for the support by the European Research Council under grant 239605. C. Mordasini acknowledges the hospitality of the Kavli Institute for Theoretical Physics at the UCSB in spring 2010 (funded by the US NSF through Grant PHY05-51164). Calculations were made on the PANSTARRS cluster at the Rechenzentrum Garching of the Max Planck Society. We thank an anonymous referee for helpful suggestions.

References

Alexander, R. D., & Armitage, P. J. 2009, ApJ, 704, 989
Alibert, Y., Mordasini, C., & Benz, W. 2004, A&A, 417, L25
Alibert, Y., Mordasini, C., Benz, W., & Winisdoerffer, C. 2005a, A&A, 434, 343
Alibert, Y., Mousis, O., Mordasini, C., & Benz, W. 2005b, ApJ, 626, L57
Alibert, Y., Mordasini, C., & Benz, W. 2010, A&A, 526, A63 (Paper III)
Ammler-von Eiff, M., Santos, N. C., Sousa, S. G., et al. 2009, A&A, 507, 523
Andrews, S. M., Wilner, D. J., Hughes, A. M., Qi, C., & Dullemond, C. P. 2009, ApJ, 700, 1502
Andrews, S. M., Wilner, D. J., Hughes, A. M., Qi, C., & Dullemond, C. P. 2010, ApJ, 723, 1241
Armitage, P. J. 2007, ApJ, 665, 1381
Baraffe, I., & Chabrier, G. 2010, A&A, 521, A44
Baumann, P., Ramírez, I., Meléndez, J., Asplund, M., & Lind, K. 2010, A&A, 519, A87
Beckwith, S. V. W., & Sargent, A. I. 1996, Nature, 383, 139
Boley, A. C. 2009, ApJ, 695, L53
Bonavita, M., Claudi, R. U., Tinetti, G., et al. 2009, AIP Conf. Ser., 1094, 429
Bouvier, J. 2008, A&A, 489, L53
Bowler, B. P., Johnson, J. A., Marcy, G. W., al. 2010, ApJ, 709, 396
Masset, F. S., & Casoli, J. 2010, ApJ, 723, 1393
Cochran, W. D., Hatzes, A. P., & Hancock, T. J. 1991, ApJ, 380, L35
Cochran, W. D., Endl, M., Wittenmyer, R. A., & Bean, J. L. 2007, ApJ, 665, 1407
Currie, T. 2009, ApJ, 694, L171
Dodson-Robinson, S. E., Laughlin, G., Bodenheimer, P., & Fischer, D. 2006, ApJ, 643, 484
Dodson-Robinson, S. E., Bodenheimer, P., Laughlin, G., et al. 2008, ApJ, 688, L99
Dodson-Robinson, S. E., Veras, D., Ford, E. B., & Beichman, C. A. 2009, ApJ, 707, 79
Dzyurkevich, N., Flock, M., Turner, N. J., Klahr, H., & Henning, T. 2010, A&A, 515, A70
Fang, M., van Boekel, R., Wang, W., et al. 2009, A&A, 504, 461
Fedele, D., van den Ancker, M. E., Henning, T., Jayawardhana, R., & Oliveira, J. M. 2010, A&A, 510, A72
Fischer, D. A., & Valenti, J. 2005, ApJ, 622, 1102
Fuhrmann, K., & Bernkopf, J. 2008, MNRAS, 384, 1563
Ghezzi, L., Cunha, K., Smith, V. V., et al. 2010a, ApJ, 720, 1290
Ghezzi, L., Cunha, K., Smith, V. V., & de la Reza, R. 2010b, ApJ, 724, 154
Gonzalez, G. 1997, MNRAS, 285, 403
Gonzalez, G. 2009, MNRAS, 399, L103
Greaves, J. S., Fischer, D. A., Wyatt, M. C., Beichman, C. A., & Bryden, G. 2007, MNRAS, 378, L1
Haisch, K. E., Lada, E. A., & Lada, C. J. 2001, ApJ, 553, L153
Hale, A. 1995, PASP, 107, 22
Han, I., Lee, B. C., Kim, K. M., et al. 2010, A&A, 509, A24
Hartmann, L., Calvet, N., Gullbring, E., & D'Alessio, P. 1998, ApJ, 495, 385
Hayashi, C. 1981, Prog. Theor. Phys. Suppl., 70, 35
Howard, A. W., Marcy, G. W., Johnson, J. A., et al. 2010, Science, 330, 653
Ida, S., & Lin, D. N. C. 2004a, ApJ, 604, 388
Ida, S., & Lin, D. N. C. 2004b, ApJ, 616, 567
Ida, S., & Lin, D. N. C. 2005, ApJ, 626, 1045
Ida, S., & Lin, D. N. C. 2008, ApJ, 673, 487
Ida, S., & Lin, D. N. C. 2010, ApJ, 719, 810
Ikoma, M., Nakazawa, K., & Emori, H. 2000, ApJ, 537, 1013
Israelian, G., Delgado Mena, E., Santos, N. C., et al. 2009, Nature, 462, 189
Kennedy, G. M., & Kenyon, S. J. 2009, ApJ, 695, 1210
Kley, W., & Dirksen, G. 2006, A&A, 447, 369
Kornet, K., Różyczka, M., & Stepinski, T. F. 2004, A&A, 417, 151
Kornet, K., Bodenheimer, P., Różyczka, M., & Stepinski, T. F. 2005, A&A, 430, 1133
Kornet, K., Wolf, S., & Różyczka, M. 2006, A&A, 458, 661
Latham, D. W., Stefanik, R. P., Mazeh, T., Mayor, M., & Burki, G. 1989, Nature, 339, 38
Lin, D. N. C., & Papaloizou, J. 1986, ApJ, 309, 846
Lissauer, J. J. 1993, ARA&A, 31, 129
Lissauer, J. J., Hubickyj, O., D'Angelo, G., & Bodenheimer, P. 2009, Icarus, 199, 338
Lodders, K. 2003, ApJ, 591, 1220
Lovis, C., & Mayor, M. 2007, A&A, 472, 657
Lubow, S. H., Seibert, M., & Artymowicz, P. 1999, ApJ, 526, 1001
Lyra, W., Paardekooper, S.-J., & Mac Low, M.-M. 2010, ApJ, 715, L6
Mamajek, E. E. 2009, AIP Conf. Ser., 1158, 3
Marcus, R. A., Sasselov, D., Hernquist, L., & Stewart, S. T. 2010, ApJ, 712, L73
Marois, C., Macintosh, B., Barman, T., et al. 2008, Science, 322, 1348
Marois, C., Zuckerman, B., Konopacky, Q. M., Macintosh, B., & Barman, T. 2010, Nature, 468, 1080
Matsuo, T., Shibai, H., Ootsubo, T., & Tamura, M. 2007, ApJ, 662, 1282
Matsuyama, I., Johnstone, D., & Hartmann, L. 2003, ApJ, 582, 893
Mayor, M., & Udry, S. 2008, Phys. Scr. T, 130, 014010
Mayor, M., Marmier, M., Lovis, C., et al. 2011, A&A, submitted [arXiv:1109.2497]
McCaughrean, M. J., & O'dell, C. R. 1996, AJ, 111, 1977
McKee, C. F., & Ostriker, E. C. 2007, ARA&A, 45, 565

Miller, N., & Fortney, J. J. 2011, ApJ, 736, L29
Min, M., Dullemond, C. P., Kama, M., & Dominik, C. 2011, Icarus, 212, 416
Mordasini, C., Alibert, Y., & Benz, W. 2009a, A&A, 501, 1139 (Paper I)
Mordasini, C., Alibert, Y., Benz, W., & Naef, D. 2009b, A&A, 501, 1161 (Paper II)
Mordasini, C., Mayor, M., Udry, S., et al. 2011a, A&A, 526, A111
Mordasini, C., Dittkrist, K.-M., Alibert, Y., et al. 2011b, in Proc. IAU Symp. 276, ed. A. Sozzetti, M. G. Lattanzi, & A. P. Boss, 72
Movshovitz, N., Bodenheimer, P., Podolak, M., & Lissauer, J. J. 2010, Icarus, 209, 616
Niedzielski, A., Nowak, G., Adamów, M., & Wolszczan, A. 2009, ApJ, 707, 768
Paardekooper, S.-J., Baruteau, C., Crida, A., & Kley, W. 2010, MNRAS, 401, 1950
Pasquini, L., Döllinger, M. P., Weiss, A., et al. 2007, A&A, 473, 979
Pollack, J. B., Hubickyj, O., Bodenheimer, P., et al. 1996, Icarus, 124, 62
Reffert, S., & Quirrenbach, A. 2011, A&A, 527, A140
Santos, N. C., Israelian, G., & Mayor, M. 2001, A&A, 373, 1019
Santos, N. C., Israelian, G., Mayor, M., Rebolo, R., & Udry, S. 2003, A&A, 398, 363
Santos, N. C., Pont, F., Melo, C., et al. 2006, A&A, 450, 825
Santos, N. C., Mayor, M., Benz, W., et al. 2010, A&A, 512, A47
Sandor, Z., Lyra, W., & Dullemond, C. 2011, ApJ, 728, L9
Schlaufman, K. C., Lin, D. N. C., & Ida, S. 2009, ApJ, 691, 1322
Scott, E. R. D. 2006, Icarus, 185, 72
Setiawan, J., Hatzes, A. P., von der Lühe, O., et al. 2003, A&A, 398, L19
Setiawan, J., Weise, P., Henning, T., et al. 2008, Precision Spectroscopy in Astrophysics, 201
da Silva, L., Girardi, L., Pasquini, L., et al. 2006, A&A, 458, 609
Sousa, S. G., Santos, N. C., Mayor, M., et al. 2008, A&A, 487, 373
Sousa, S. G., Fernandes, J., Israelian, G., & Santos, N. C. 2010, A&A, 512, L5
Sousa, S. G., Santos, N. C., Israelian, G., Mayor, M., & Udry, S. 2011, A&A, 533, A141
Sozzetti, A. 2004, MNRAS, 354, 1194
Sozzetti, A., & Desidera, S. 2010, A&A, 509, A103
Syer, D., & Clarke, C. J. 1995, MNRAS, 277, 758
Tanaka, H., Takeuchi, T., & Ward, W. R. 2002, ApJ, 565, 1257
Thommes, E. W., Matsumura, S., & Rasio, F. A. 2008, Science, 321, 814
Udry, S., & Santos, N. C. 2007, ARA&A, 45, 397
Udry, S., Mayor, M., Naef, D., et al. 2000, A&A, 356, 590
Udry, S., Mayor, M., Naef, D., et al. 2002, A&A, 390, 267
Udry, S., Mayor, M., Benz, W., et al. 2006, A&A, 447, 361
Valenti, J. A., & Fischer, D. A. 2008, Phys. Scr. T, 130, 014003
Veras, D., & Armitage, P. J. 2004, MNRAS, 347, 613
Wyatt, M. C., Clarke, C. J., & Greaves, J. S. 2007, MNRAS, 380, 1737